Journal of Vibration Engineering & Technologies (2023) 11:1241–1270
https://doi.org/10.1007/s42417-022-00639-0

ORIGINAL PAPER

Free Flexural Vibration Analysis of Thin Plates Using NURBS-Augmented Finite-Element Method

Biraja Prasad Mishra[1] · **Manoranjan Barik**[2]

Received: 30 March 2022 / Revised: 21 June 2022 / Accepted: 6 July 2022 / Published online: 9 August 2022

Abstract

In isogeometric analysis (IGA), the non-uniform rational B-spline (NURBS) basis functions are used for depicting the geometry and the displacement field. As the NURBS basis functions are non-interpolating in nature, the enforcement of essential boundary condition becomes a difficult task. In order to circumvent the above problem, recently the authors Mishra and Barik (Comput 232:105869, 2020; Eng Comput 35:351–362, 2019) proposed a new method called NURBS-augmented finite-element method (NAFEM). The authors have incorporated the non-uniform rational B-spline (NURBS) basis functions for the representation of the geometry and the usual finite-element basis functions are adopted for the field variables as they satisfy the Kronecker-Delta property. This simplifies the implementation of the boundary condition to a great extent. In the present work, NAFEM is extended for free vibration analysis of plates having different geometries and boundary conditions, and the results are found to be in excellent agreement with the existing ones. To showcase the robustness of NAFEM, some arbitrary-shaped plates have also been considered, and the new results are presented.

Keywords NURBS-augmented finite-element method (NAFEM) · Finite-element analysis (FEA)

Introduction

The finite-element analysis (FEA) is applied to many disciplines where engineering structures are concerned. The structure's geometry plays a significant role in the analysis and hence its accurate representation is inevitable for more realistic analysis. The challenge faced by the researchers to deal with the analysis of plates of various geometrical configurations steered to develop many methods and techniques. Some researchers proposed techniques for dealing with multiple planforms when some of the investigators proposed to analyze a particular shape of the plate.

A semi-analytic approach is suggested for free vibration analysis of annular sector plates [3]. The subparametric concept is used in the spline finite-strip method to examine plates of general shape for static and free vibration analyses [4]. Vibration analysis of plates of general quadrilateral and sectorial planforms is carried out by applying the differential quadrature method using the geometric mapping technique [5]. Kirchhoff plates of arbitrary shape have been studied for free vibration using the mapping technique in the finite-element method [6, 7].

The free vibration analysis of plates of different geometries is presented by Lee [8] using a four-noded plate element. He has considered the natural strains based on Reissner–Mindlin assumptions taking account of the shear deformation and rotatory inertia effect. Shear-deformable plates of different geometrical configurations for free vibration and buckling analyses have been reported employing the mesh-free method based on the reproducing kernel particle approximate [9]. The vibration of several structural models such as rods, thin beams, membranes, and thin plates are studied by Cottrell et al. [10] using isogeometric analysis (IGA). The authors have considered the rotationless beams and plates as three-dimensional solid models and used the knot refinement concept to get more accurate and robust

✉ Biraja Prasad Mishra
birajaprmishra@gmail.com

Manoranjan Barik
manoranjanbarik@yahoo.co.in

[1] Department of Civil Engineering, Madanapalle Institute of Technology & Science, Angallu, Madanapalle, Andhra Pradesh 517326, India

[2] Department of Civil Engineering, National Institute of Technology Rourkela, Sundergarh, Rourkela, Odisha 769008, India

results than the corresponding finite elements. Reali [11] applied the concept of IGA to study the response of one-dimensional and two-dimensional problems under vibration.

The amalgamation of the subparametric triangular plate bending element with first-order shear deformation theory for the analysis of a square plate with a circular cut-out at the center is described in [12]. The NURBS-enhanced finite-element method (NEFEM) [13] is an improvement to the classical finite-element method. This method can represent the geometry precisely through computer-aided design (CAD) description of the boundary with NURBS. In this technique, the elements which do not intersect the edge require a standard finite-element interpolation function and numerical integration for the analysis. In contrast, the elements which cross the NURBS boundary require a specially designed piecewise polynomial interpolation function and numerical integration. The authors have studied the application of NEFEM to $2D$ Poisson problems and electromagnetic scattering simulation showing its advantages compared to the classical isoparametric finite-element formulation. A family of elements of smooth, curved geometry using rational Bézier functions for boundary description has been introduced by Lu [14] by which the common shapes such as circles and ellipses are described precisely. These elements are suited for analyzing discrete bodies undergoing more or less uniform or regular deformation.

Irregular shapes thin plates for free vibration have been analyzed by quadrature element method (QEM) [15, 16]. Free vibration analysis of annular sector plates and graphene sheets is performed using eight-node curvilinear domains in discrete singular convolution (DSC) method [17, 18].

The direct imposition of inhomogeneous essential boundary conditions to the NURBS control points is found to be problematic, leading to significant errors with deteriorated rates of convergence [19]. Therefore, the investigators have represented an improved formulation for NURBS-based isogeometric analysis by employing a transformation method to the boundary points, which relates the control variables to the collocated nodal values at the essential boundary. Using the open knot vectors, the resulting NURBS basis functions associated with control points vanish at the periphery. Bazilevs et al. [20] explored T-splines, which is a generalization of NURBS enabling local refinement, as a basis for IGA. The researchers have applied bivariate and trivariate T-splines of various degrees to elementary fluid and structural mechanics problems. Hughes et al. [21] have initiated the study of efficient quadrature rules for NURBS-based isogeometric analysis. A rule of thumb known as the half-point rule has emerged, indicating that optimal rules involve several points roughly equal to half the number of degrees-of-freedom or equivalently half the number of basis functions of the space under consideration. The half-point rule is independent of the polynomial order of the basis.

The Dirichlet boundary conditions in IGA can be suitably imposed by taking the quasi-interpolation methods into account [22]. de Falco et al. [23] have developed GeoPDEs, which is a suite of free software tools for applications of IGA focusing on providing a common framework for the implementation of the many IGA methods for the discretization of currently studied partial differential equations, mainly based on B-splines and NURBS. Different geometric Kirchhoff plates have been undertaken for free vibration analysis by a moving Kriging interpolation-based mesh-free method [24]. Schmidt et al. [25] have presented a methodology enabling IGA on trimmed NURBS surfaces. A local reconstruction technique using a geometric basis has been developed and applied to evaluate the finite-element constituents of the trimmed knot spans in terms of the underlying control variables. The Lagrange multiplier method to impose the essential boundary conditions for improving the accuracy of the solution in the IGA of thin plates has been used in [26].

The isogeometric static, dynamic, and buckling analyses of rectangular and circular-shaped functionally graded material (FGM) plates for different boundary conditions have been carried out by Tran et al. [27]. Here, higher order shear deformation theory (HSDT) model is developed using C^1 continuous elements to improve the accuracy of the solution and taking the stress distribution without using shear correction factors. Blending NURBS with Lagrangian representations in IGA has been first developed by Lu et al. [28]. In the blended representation, selected boundary edges or surfaces of a multivariate NURBS patch are parametrized in (rational) Lagrangian form. The Lagrangian parameters are obtained by transforming the NURBS representation. The transformation, by construction, exactly preserves the original geometry, which is helpful in interfacing the NURBS domain to finite element domains or for imposing essential boundary conditions.

The bending, free flexural vibration, buckling, and flutter behavior of square and skew functionally graded material (FGM) plates under different boundary conditions using NURBS-based finite element is being studied by Valizadeh et al. [29]. Further, the isogeometric finite-element analysis is incorporated with refined plate theory to study the behavior of functionally graded material square and circular plates for static, free vibration and buckling analyses in [30] where displacement field is approximated with four degrees-of-freedom per each control point allowing an efficient solution process. The isogeometric locking free plate formulation for the bending, buckling, and free vibration analyses of homogeneous and functionally graded square, circular and square plates with complicated cut-out considering different boundary conditions and gradient index is adopted in [31]. Jüttler et al. [32] have initiated G+SMO (Geometry+Simulation Modules), an open-source, C++ library for IGA. It is an object-oriented template library that implements a generic

concept for IGA, based on abstract classes for discretization basis, geometry map, assembler, solver, and using the object polymorphism and inheritance techniques to provide a common framework of IGA for a variety of different available basis types. Nguyen and Nguyen-Xuan [33] have proposed an efficient computational tool based on isogeometric finite-element formulation of three-dimensional elasticity for static and dynamic response of functionally graded square, circular, annular, and square plates with complicated shaped cut-outs. The numerical tests have shown that a quartic NURBS element can eliminate the shear-locking phenomena. An effective formulation combining the extended-isogeometric approach and higher order shear deformation theory for free vibration analysis of cracked functionally graded material plates is presented by Tran et al. [34]. This formulation accounts for the effects of gradient index, crack-length, crack-location, length-to-thickness ratio on the natural frequencies and mode shapes of simply supported and clamped FGM plates.

Vázquez [35] has presented a new design for the implementation of IGA in Octave and MATLAB package for the solution of partial differential equations. Compared to the previous version [23], the new design is more efficient in terms of memory consumption and computational time. Massarwi and Elber [36] have developed tools for approximation and local re-parameterization of trimmed elements for three-dimensional problems based on volumetric modeling via volumetric representations (V-reps). A differential quadrature hierarchical finite-element method (DQHFEM) is proposed for vibration, and bending analyses of Mindlin plates with curvilinear domains [37]. The non-uniform rational Lagrange (NURL) alternative basis, which are interpolation functions to represent NURBS geometries for IGA, has been reported in [38]. The authors have incorporated the same basis functions to carry out the in-plane and flexural vibration of thin plates to overcome the difficulties of IGA using NURBS on coping with Dirichlet boundary conditions. Free vibration analysis of conical and cylindrical shells and annular plates made of composite, functionally graded materials (FGM), and carbon nanotube reinforced (CNTR) composite using FSDT via discrete singular convolution method is carried out in [39]. A comprehensive review on trimming in IGA has been showcased in [40] in the context of design, data exchange, and computational simulation. Employing the Fourier expansion method, sector-like thin plates having simply supported radial edges have been analyzed for transverse vibration adopting a semi-analytical approach [41]. Antolin et al. [42] have demonstrated a novel approach for the construction of isogeometric numerical methods for elliptic PDEs on trimmed geometries. Improved Fourier series method (IFSM) is used by Liu et al. [43] for free in-plane vibration of arbitrarily shaped straight-sided quadrilateral and triangular plates. They have solved the problems by mapping the arbitrarily shaped plates into a unit square plate and following the usual modeling of vibration problems for rectangular plates. Alihemmati and Beni [44] have proposed a mesh-free Galerkin method for analysis of plates of triangular and polygonal geometries. Recently, Sahoo and Barik [45–47] have analyzed curved and straight-edged stiffened plates for free vibration and dynamic response to moving loads. They have employed an isoparametric finite element with shear deformation to accomplish this task.

The aero-thermo-elastic panel flutter response of a functionally graded plate having cracks in the supersonic flow field has been analyzed by Khalafi and Fazilati [48]. The authors have incorporated IGA along with Nitsche technique which based is on FSDT. The parametric instability response of laminated composite plates under uniform in-place loading has been carried out for the first time in [49]. Here, the authors have incorporated the IGA-based FEM formulation for addressing the instability of the panels. The response of a perforated flat panel having an externally bonded two-steered patch of variable stiffness has been presented in [50]. Khalafi and Fazilati [51] studied the free vibration of a repaired perforated plate. They have incorporated the FSDT of plates for the multi-patch modeling approach. The free vibration and linear flutter analyses of laminated square and skew shaped plates have been carried out in [52]. The formulation is based on the FSDT in-conjunction with an aerodynamic loading model. Free vibration analysis of laminated composite plates having curved perforations has been extensively reported in [53]. The researchers have considered an IGA formulation with Nitsche method using FSDT. Liu et al. [54] proposed the in-plane free vibration of arbitrary plates having various end conditions using Improved Fourier Series Method (IFSM). Here, the authors have mapped the plates to a unit square plate and the usual procedure adopted in case of rectangular plates is used for the solution. A NURBS-based multi-patch IGA formulation with FSDT has been presented in [55]. Do and Lee [56] studied the free vibration response of FGM plates with cut-outs by incorporating IGA. Here, the authors have formulated a quasi-3D higher order shear deformation theory(HSDT).

The researchers continuously endeavor to have analytical solutions to the arbitrary shape thin-plate analysis. But the analytical expressions become too complex and unmanageable when it is attempted for plates having curved edges and other than rectangular or straight-sided planforms. In the numerical method of analysis, FEM was predominant so far in formulating new elements to model the arbitrary shape of the plates. Isoparametric element was considered a successful one in dealing with the non-rectangular plate geometries, though it is deficient in describing the exact curved edges. Moreover, as this element is based on Mindlin's theory, the shear strain term leads to the shear-locking problem when

applied to thin plates and needs special attention of reduced integration.

There was a significant change of approach when the Computer-Aided Design (CAD) was developed to represent the geometry accurately, and this was embedded into FEA [57] through the concept of IGA, where the researchers employed the NURBS basis functions for representation of the geometry as well as the field variables required for the analysis. As the NURBS basis functions are non-interpolating in nature, the enforcement of essential boundary condition was found to be difficult and seeks special treatment [58–64].

In the present work, the above mentioned boundary condition imposition problem is alleviated by replacing the NURBS with classical finite-element basis function to represent the field variables. The NURBS basis functions are only used for describing the geometry, and the four-noded *ACM (Adini, Clough and Melosh* [65]) plate bending element having 12 degrees of freedom is considered for the displacement field. The interpolating nature of the *ACM* plate bending element helps in enforcing the essential boundary condition similar to the classical finite element method, making the whole process simpler. The NAFEM has been successfully applied to analyses of arbitrarily shaped plates [1, 2, 66, 67]. The present work is an extension of NAFEM for analyzing plates of different planforms under various end conditions for free vibration.

Problem Statement

The equation of equilibrium for an elastic system under free vibration in matrix form is given by

$$[K]\{\delta\} + [M]\left\{\ddot{\delta}\right\} = \{0\}, \tag{1}$$

where $[K]$ is the global elastic-stiffness matrix, $[M]$ is the global consistent mass matrix, $\{\delta\}$ is the displacement vector, $\left\{\ddot{\delta}\right\}$ is the acceleration vector. Equation (1) can be solved using the standard matrix analysis once the element matrices are assembled into the global matrices.

Finite-Element Formulation

NURBS Basis Function

Given a knot vector $S = \left\{s_1, s_2, s_3, \ldots s_{n+p+1}\right\}$, the associated set of B-spline basis functions $\left\{N_{i,p}\right\}_{i=1}^{n}$ are defined recursively by the Cox–de-Boor formula [68], starting with the zeroth order basis function ($p = 0$) as

$$N_{i,0} = \begin{cases} 1 \text{ if } s_i \le s \le s_{i+1} \\ 0 \text{ otherwise,} \end{cases} \tag{2}$$

and for a polynomial order $p \ge 1$

$$N_{i,p}(s) = \frac{s - s_i}{s_{i+p} - s_i} N_{i,p-1}(s) + \frac{s_{i+p+1} - s}{s_{i+p+1} - s_{i+1}} N_{i+1,p-1}(s), \tag{3}$$

where n is the number of basis functions and p is the order of the basis functions. The fractions of the form 0/0 are defined as zero.

Mapping of the Plate

The use of NURBS basis functions for representation of geometry introduces the concept of parametric space which is absent in the conventional finite-element formulation [68]. The consequence of this additional space is that an additional mapping is performed to operate in the parent element coordinates. First, the parent space is mapped to the parametric space and then to the physical space (Fig. 1).

The mapping from parametric to physical space is given by

$$[X] = \sum_{i=1}^{n} \sum_{j=1}^{m} P_{i,j} R_{i,j}^{p,q}(s,t), \tag{4}$$

where p and q are the order, n and m are the number of control points, $P_{i,j}$ are the control points and $R_{i,j}^{p,q}(s,t)$ is the bivariate NURBS basis function defined as

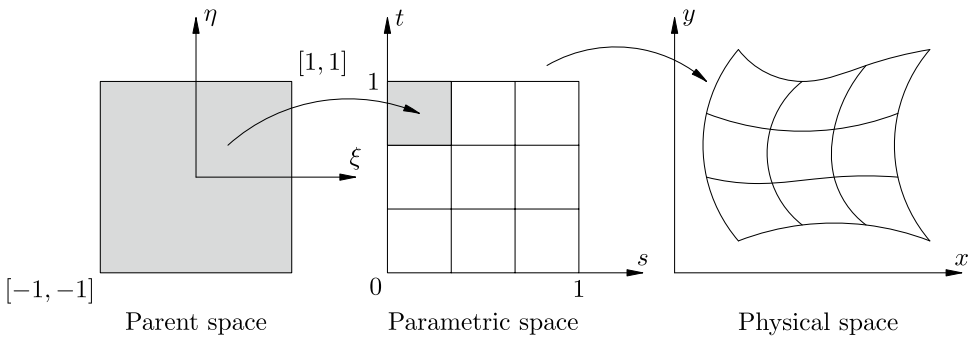

Fig. 1 Mapping between domains/spaces

$$R_{i,j}^{p,q}(s,t) = \frac{N_i(s)M_j(t)w_{i,j}}{\sum_{\bar{i}=1}^{n}\sum_{\bar{j}=1}^{m} N_{\bar{i}}(s)M_{\bar{j}}(t)w_{\bar{i},\bar{j}}}, \tag{5}$$

where $N_i(s)$ and $M_j(t)$ are the univariate B-spline basis functions of order p and q corresponding to the knot vectors in the respective directions and $\{w_{i,j}\}_{i=1,j=1}^{n,m}$, where $w_{i,j} > 0$ are the set of NURBS weights. The mapping from parent to parametric space is given by [68]

$$s(\xi) = \frac{(s_{i+1} - s_i)\xi + (s_{i+1} - s_i)}{2} \tag{6}$$

$$t(\eta) = \frac{(t_{i+1} - t_i)\eta + (t_{i+1} - t_i)}{2}. \tag{7}$$

For complex geometries the physical space may be divided into simple patches and then those patches are mapped to the parent space through the parametric space. As a typical example the physical space defined by the coordinates ACDB is divided into two patches namely ACFE and EFDB as shown in Fig. 2. The parent space is then mapped to the patches in the physical space through the parametric space and the procedure is followed as before to compute the stiffness matrix of each patch. The stiffness matrices of all the patches are assembled to form the global stiffness matrix of the whole plate. Thus the analysis of the plates having complicated geometry can be made simpler by subdividing them into more amenable patches which can be dealt with ease [1].

Mesh Generation

The mesh for the plate is generated using the knot refinement technique of [68]. In this, the plate geometry is generated first using the NURBS (Fig. 3a), and then applying the *h*-refinement technique [23, 68], the desired meshes can be obtained. Figure 3 shows the different stages of mesh generation for a typical semi-circular semi-elliptical plate which has also been used as an example problem in this paper. For detail of this technique, Section 2.1.4 of [69] may be referred.

Displacement Interpolation Function

For the proposed element, the four-noded rectangular non-conforming *ACM* plate bending element with 12 degrees-of-freedom is taken as the basic element. As the element is in ξ-η plane the shape functions and the nodal parameters for the displacements and slopes are expressed in terms of the coordinates $\xi - \eta$ unlike the $x - y$ coordinates of the parent *ACM* element [6]. The shape functions for the displacement field for the jth node are given as

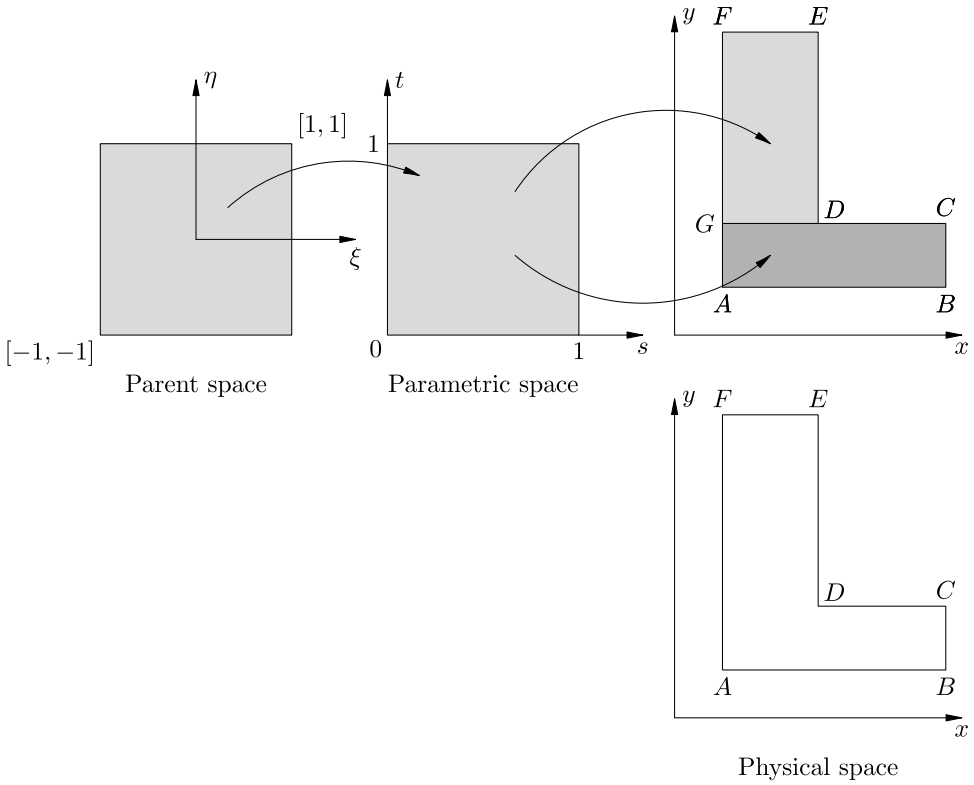

Fig. 2 Mapping of complex shaped geometry through different domains/spaces

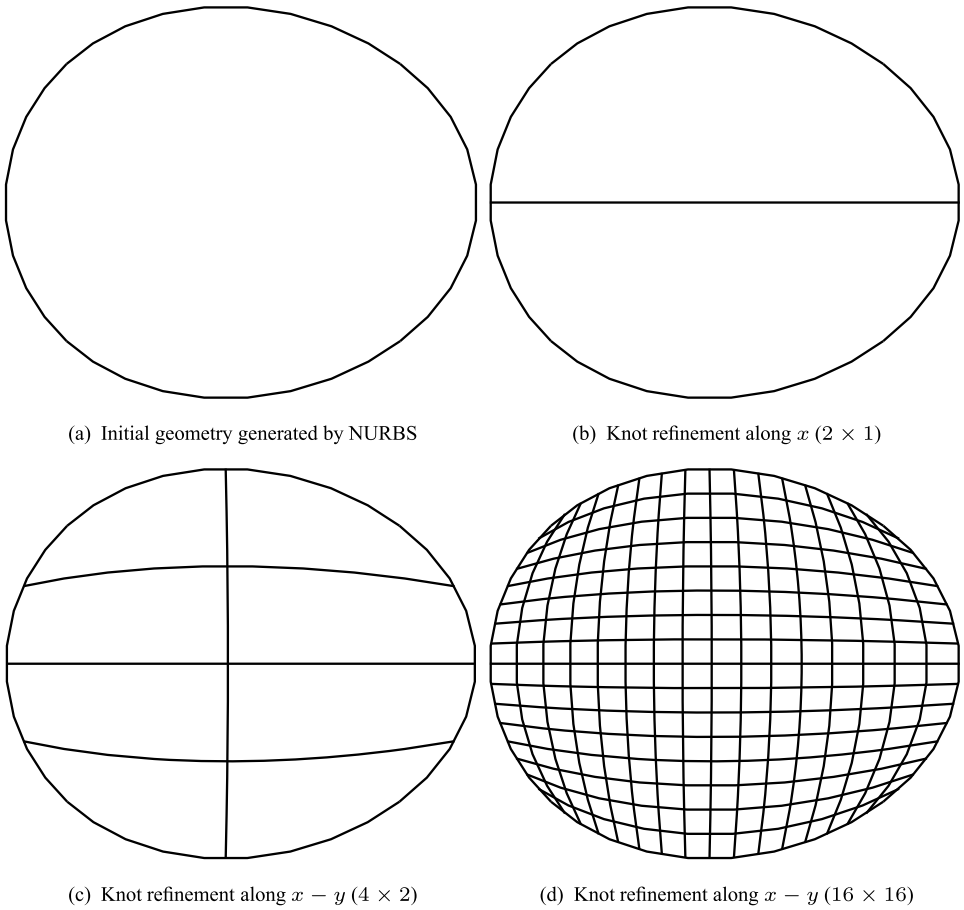

(a) Initial geometry generated by NURBS (b) Knot refinement along x (2×1)

(c) Knot refinement along $x - y$ (4×2) (d) Knot refinement along $x - y$ (16×16)

Fig. 3 Mesh generation of a typical semi-circular semi-elliptical plate

$$\left[N_w^j \; N_{\theta_\xi}^j \; N_{\theta_\eta}^j\right] = \frac{1}{8} \times \begin{bmatrix} (s_0+1)(t_0+1)\left(2+s_0+t_0-\xi^2-\eta^2\right) \\ s_j(s_0+1)^2(s_0-1)(t_0+1) \\ t_j(s_0+1)(t_0+1)^2(t_0-1) \end{bmatrix}^T, \tag{8}$$

where $s_0 = \xi s_j$ and $t_0 = \eta t_j$.

The detailed formulation is presented in Section 2.4 of [1, 2].

Strain–Displacement Matrix

The strain–displacement matrix is given by $[B] = [T][\bar{B}]$, where $[\bar{B}] = \left[\frac{\partial N_w}{\partial \xi} \; \frac{\partial N_w}{\partial \eta} \; \frac{\partial^2 N_w}{\partial \xi^2} \; \frac{\partial^2 N_w}{\partial \eta^2} \; \frac{\partial^2 N_w}{\partial \xi \, \partial \eta}\right]^{\mathrm{T}}$ and $[T] = \left[[T_{F_1}] \; [T_{F_2}]\right]$; $[T_{F_1}] = -[J6]^{-1}[J5][J4]^{-1}[J1]^{-1}$, $[T_{F_2}] = [J6]^{-1}[J3]^{-1}$.

The detail formulation of the above can be referred from Section 2.5 of [1, 2].

Stiffness Matrix

Total potential energy of the plate element is given by

$$\Pi_p = \frac{1}{2} \iint \left\{\epsilon(x,y)\right\}^{\mathrm{T}} \left\{\sigma(x,y)\right\} \mathrm{d}x \, \mathrm{d}y - \iint w^{\mathrm{T}} \mathrm{d}x \, \mathrm{d}y. \tag{9}$$

Applying the principle of minimum potential energy and making appropriate substitutions for strain vector ($\left\{\epsilon(x,y)\right\}$), the stress vector ($\left\{\sigma(x,y)\right\}$) and the displacement field (w—Eq. (8) of [1]), we have

$$[K]_e \left\{\delta\right\} = \left\{P\right\}_e, \tag{10}$$

where $\left\{\delta\right\}$ is the vector of nodal displacements, $\left\{P\right\}_e$ is the vector of nodal forces and $[K]_e$ is the plate element stiffness matrix given by

$$[K]_e = \iint [B]^{\mathrm{T}}[D][B] \, \mathrm{d}x \, \mathrm{d}y. \tag{11}$$

Since the NURBS basis is a function of s and t, Eq. (11) becomes

$$[K]_e = \iint [B]^{\mathrm{T}}[D][B] \left|J4\right| \,\mathrm{d}s\,\mathrm{d}t. \tag{12}$$

Again since $[B]$ is a function of ξ and η, Eq. (12) becomes

$$[K]_e = \iint [B]^{\mathrm{T}}[D][B] \left|J1\right| \left|J4\right| \,\mathrm{d}\xi\,\mathrm{d}\eta. \tag{13}$$

The integration is carried out numerically by adopting 2×2 Gaussian quadrature formula.

Consistent Mass Matrix

Reproducing the procedures adopted in [7], the consistent mass matrix of the plate element is formulated on the basis of the lateral displacement w. The acceleration of a point in the middle plane of the plate in terms of the interpolation function given in Sect. 2.4 of [1, 2] can be expressed as

$$\left\{\ddot{f}\right\} = \left\{\ddot{w}\right\} = \left[N_w\right]\left\{\ddot{\delta}\right\}. \tag{14}$$

Hence, the inertia force for a small volume $\mathrm{d}V$ at that point is given by

$$\left\{f_I\right\} = \rho\,\mathrm{d}V\left[N_w\right]\left\{\ddot{w}\right\} = \rho\,\mathrm{d}V\left[N_w\right]\left\{\ddot{\delta}\right\}. \tag{15}$$

where ρ is the mass density of the plate material. If $\left\{F_I\right\}$ is the nodal inertia force parameter, then the contribution of inertia in the equation of motion can be obtained from the principle of virtual work and can be expressed as

$$\left\{\mathrm{d}\delta^{\mathrm{T}}\right\}\left\{F_I\right\} = \int_v \left\{\mathrm{d}f^{\mathrm{T}}\right\}\left\{f_I\right\}. \tag{16}$$

The above equation with the help of Eq. (15) can be rewritten as

$$\begin{aligned}&\left\{\mathrm{d}\delta^{\mathrm{T}}\right\}\left\{F_I\right\}\\ &\quad= \int_v \{d\delta^T\}\left[N_w\right]\rho\,dV\{\ddot{\delta}\}\end{aligned} \tag{17}$$

from which

$$\begin{aligned}\{F_I\} &= \rho\int_v \left[N_w\right]^{\mathrm{T}}\left[N_w\right]\mathrm{d}V\{\ddot{\delta}\}\\ &= [M]_e\{\ddot{\delta}\},\end{aligned} \tag{18}$$

where $[M]^e$ is the mass matrix of the bare plate element and for constant thickness t, it is given by

$$\begin{aligned}[M]_e &= \rho\int_v [N_w]^{\mathrm{T}}[N_w]\,\mathrm{d}V = \rho\,t\int\int [N_w]^{\mathrm{T}}[N_w]\,\mathrm{d}x\,\mathrm{d}y\\ &= \rho\,t\int\int [N_w]^{\mathrm{T}}[N_w]\left|J4\right|\,\mathrm{d}s\,\mathrm{d}t\\ &= \rho\,t\int\int [N_w]^{\mathrm{T}}[N_w]\left|J1\right|\left|J4\right|\,\mathrm{d}\xi\,\mathrm{d}\eta.\end{aligned} \tag{19}$$

Boundary Conditions

Following the procedure similar to the case of static and buckling analysis [1, 2], the stiffness of the boundary is given by

$$[K_b] = \int [N_b]^T[N_k]\left|J_b\right|\,\mathrm{d}\lambda_1, \tag{20}$$

where

$$[N_b] = \begin{bmatrix}1 & 0 & 0\\ [10pt]0 & \cos\beta & \sin\beta\\ [10pt]0 & -\sin\beta & \cos\beta\end{bmatrix}\begin{Bmatrix}[N_w]\\ [8pt]\dfrac{\partial[N_w]}{\partial x}\\ [10pt]\dfrac{\partial[N_w]}{\partial y}\end{Bmatrix} \tag{21}$$

$$= \begin{bmatrix}k_w & 0 & 0\\ [10pt]0 & k_\alpha\cos\beta & k_\alpha\sin\beta\\ [10pt]0 & -k_\beta\sin\beta & k_\beta\cos\beta\end{bmatrix}\begin{Bmatrix}[N_w]\\ [10pt]\dfrac{\partial[N_w]}{\partial x}\\ [8pt]\dfrac{\partial[N_w]}{\partial y}\end{Bmatrix} \tag{22}$$

and Jacobian,

$$\left|J_b\right| = \frac{\mathrm{d}s_1}{\mathrm{d}\lambda_1}. \tag{23}$$

This boundary stiffness matrix contributes to that element to which the boundary belongs to.

Solution Procedure

The solution procedure adopted in the free vibration analyses of plates are presented in this section. The equilibrium equation for the free vibration is given by Eq. (1). Considering the motion as harmonic motion, the solution of Eq. (1) is

$$\{\delta\} = H\{\psi\}e^{i\omega t}, \tag{24}$$

where $\{\psi\}$ is a normalized vector of the order of $\{\delta\}$, H is the weighting parameter of $\{\psi\}$ and ω is the natural frequency of vibration in radians per second. On substitution, the equilibrium equation becomes

$$[K]\{\psi\} = \omega^2[M]\{\psi\}. \tag{25}$$

This is a generalized eigenvalue problem and is solved by the simultaneous iteration algorithm of [70] and its solution is the eigenvalue ω^2 and the eigenvector $\{\psi\}$. The skyline [71] technique is adopted for the storage of global elastic-stiffness matrix $[K]$ and the mass matrix $[M]$. In this process of storage, the matrix is stored in a single array eliminating the zero entries if any within the band thus reducing the storage requirement of the computer.

Numerical Examples

The free vibration analyses of a number of plates having different shapes and boundary conditions are carried out using the simultaneous iteration algorithm of [70] and the results obtained are compared with the existing ones. The results are presented in tabular form with a mesh division of 32×32 for the whole plate. Figures of typical plates showing mesh divisions of 8×8 along with the nodes (asterisk) are presented for each case. The abbreviations used in the table for the boundary conditions (S—simply supported, C—clamped, and F—free) are depicted in the anti-clockwise direction starting from the left edge of the plate.

Rectangular Plates

The convergence study for the different mesh sizes for the simply supported and clamped rectangular plate of aspect ratio 1 (square plate) is presented in Table 1 where excellent convergence of results is obtained with increasing mesh divisions of the plate. The free vibration results of rectangular plates having aspect ratios 0.4, 1.0, 1.5 and 2.5 and under different support conditions are presented in Table 2. The results are compared with that of analytical method [72] and they are found to be in excellent agreement. First ten natural frequency results of a simply supported rectangular plate having different thicknesses have been presented in Table 3. In another case, the effect of thickness to width ratio (h/b) on the natural frequencies of antisymmetric modes of a rectangular plate have has presented in Table 4. The present results are in excellent agreement with Classical Plate Theory (CPT [73]) and that of Lim et al. [74]. The variation of the natural frequency with respect to the change in thickness to breadth (h/b ratio) is found to be negligible. A typical rectangular plate having 8×8 mesh is shown in Fig. 4. It is observed that the frequency parameter increases with the increase in aspect ratio. The frequency parameter is found to be more for the all edges clamped plate in comparison to other support conditions. The first four mode shapes for rectangular plates under simply supported and clamped conditions are shown in Figs. 5, 6, 7, 8, 9, 10, 11 and 12.

Free Vibration of Circular Plates

The free vibration analysis of circular plates (Fig. 13) with three different boundary conditions (completely free, simply supported and clamped) are carried out and the results compared in Tables 5, 6 and 7 with the published ones are found to be in well agreement. It is observed that the dimensionless natural frequencies of a fully clamped circular plate is more in comparison to a simply supported and completely free circular plates.

Table 1 Convergence study for dimensionless natural frequencies $\left(\beta_1 = (\omega^2 a^4 \rho h/D)^{\frac{1}{4}}\right)$ of a rectangular plate under different boundary condition (aspect ratio $a/b = 1$)

	Mesh	B^*	1	2	3	4	5	6
Clamped end		[72]	35.992	73.413	73.413	108.27	131.64	132.24
	2×2	Present	32.039	86.689	86.693	4454.9	4638.7	4738.5
	4×4		34.188	69.099	69.099	95.444	120.18	121.9
	8×8		35.446	71.989	71.991	103.55	129.16	130.05
	16×16		35.844	73.017	73.02	106.92	130.89	131.56
	32×32		35.949	73.32	73.328	107.89	131.4	132.04
Simply supported		[72]	19.7392	49.3480	49.3480	78.9568	98.6960	98.6960
	2×2	Present	17.71	45.536	45.789	45.789	71.041	72.286
	4×4		19.136	47.192	47.192	71.276	94.454	94.497
	8×8		19.578	48.728	48.728	76.562	97.406	97.408
	16×16		19.698	49.189	49.189	78.314	98.366	98.342
	32×32		19.729	49.307	49.308	78.793	98.61	98.634

B^* method

Table 2 Dimensionless natural frequencies $\left(\beta_1 = (\omega^2 a^4 \rho h/D)^{\frac{1}{4}}\right)$ of a rectangular plate under different boundary condition

A^*	a/b	B^*	1	2	3	4	5	6
D^*	0.4	N^*	23.626	27.732	35.275	46.466	61.292	63.064
		M^*	23.646	27.817	35.446	46.702	61.554	63.100
	1.0	N^*	35.949	73.32	73.328	107.89	131.4	132.04
		M^*	35.992	73.413	73.413	108.27	131.64	132.24
	1.5	N^*	60.702	93.667	148.63	149.36	178.99	226.99
		M^*	60.772	93.860	148.82	149.74	179.66	226.92
	2.5	N^*	147.67	173.31	220.46	290.5	382.68	394.85
		M^*	147.80	173.85	221.54	291.89	384.71	394.37
E^*	0.4	N^*	11.441	16.16	24.043	35.057	41.026	45.673
		M^*	114.4487	16.1862	24.0818	35.1358	41.0576	45.7950
	1.0	N^*	19.729	49.308	49.321	78.814	98.611	98.604
		M^*	19.7392	49.3480	49.3480	78.9568	98.6960	98.6960
	1.5	N^*	32.058	61.622	98.619	110.9	128.02	177.06
		M^*	32.0762	61.6850	98.6960	111.0330	128.3049	177.6529
	2.5	N^*	71.508	101.0	150.2	219.11	256.44	285.46
		M^*	71.5564	101.1634	150.5115	219.5987	256.6097	286.2185
G^*	0.4	N^*	3.5	4.7603	8.0723	13.801	21.536	23.046
		M^*	3.5107	4.7861	8.1146	13.882	21.638	23.731
	1.0	N^*	3.4711	8.5051	21.289	27.195	30.955	54.166
		M^*	3.4917	8.5246	21.429	27.331	31.111	54.443
	1.5	N^*	3.4534	11.661	21.468	39.328	53.542	61.627
		M^*	3.4772	11.676	21.618	39.492	53.876	61.994
	2.5	N^*	3.4279	17.963	21.396	57.226	60.127	105.95
		M^*	3.4562	17.998	21.563	57.458	60.581	106.54

A^* support condition, B^* method, D^* CCCC, E^* SSSS, G^* CFFF

N^* present, M^* Leissa [72]

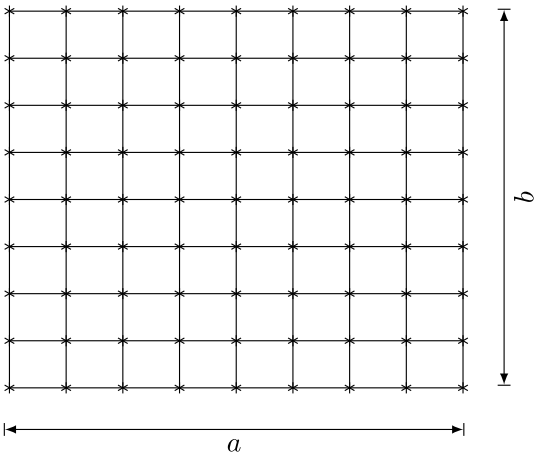

Fig. 4 A typical rectangular plate with having 8 × 8 mesh

Free Vibration of Skew Rhombic Plates

Skew rhombic plates (Fig. 14) having different skew angles (α anti-clockwise from y-axis, aspect ratio a/b = 1.0) and support conditions are analyzed and the results are presented in Tables 8, 9 an 10 with a mesh division of 32 × 32 and the results are compared with those of [6, 58] and they agree well. From the results, it is observed that the frequency parameter for a skew rhombic plate increases with the skew angle and is highest under fully clamped condition. The first four mode shapes of skew rhombic plate having skew angle $\theta = 30°$ for simply supported and SCSC boundary conditions are presented in Figs. 15, 16, 17, 18, 19, 20, 21 and 22.

Annular Sector Plate

The free vibration analysis of an annular sector plate (Fig. 23) having sector angle $\alpha = 90°$, with different aspect ratios (r_i/r_o, r_i—inner radius, r_o—outer radius) and under different boundary conditions is carried out. The results obtained are presented in Tables 11, 12 are found to be in excellent agreement with Barik [7] than Mukhopadhyay [3]. It is observed that the frequency parameter for an annular sector plate is highest under fully clamped condition. The first four mode shapes of annular sector plates having aspect ratio $r_i/r_o = 0.25$ under CSSS and simply supported boundary conditions are presented in Figs. 24, 25, 26, 27, 28, 29,

Table 3 First ten natural frequencies of a simply supported rectangular plate having different thickness (Young's modulus $E = 70 \times 10^9$ N/m^2, density $\rho = 2700$ kg/m^3, Poisson's ratio $\nu = 0.3$, length of plate = 0.6 m, breadth of plate = 0.4 m)

Mode	Thickness of plate = 0.00625 m			Thickness of plate = 0.0125 m		
number	Exact	Present	[75]	Exact	Present	[75]
1	136.5	136.49	135.8	273.1	272.97	271.7
2	262.6	262.36	259.9	525.2	524.71	519.8
3	420.1	420.01	417.6	840.3	840.03	835.2
4	472.7	472.16	466.8	945.4	944.33	933.7
5	546.2	545.03	535.9	1092.5	1090.1	1071.9
6	756.35	753.82	733.7	1512.7	1507.6	1467.5
7	766.85	766	757.1	1533.7	1532	1514.4
8	892.9	892.37	888.3	1785.8	1784.7	1776.6
9	1018.9	1016.2	997.8	2037.9	2032.5	2024.2
10	1050.4	1046.3	1012.1	2100.9	2092.5	2263.4
Mode	Thickness of plate = 0.025 m			Thickness of plate = 0.05 m		
number	Exact	Present	[75]	Exact	Present	[75]
1	546.2	545.95	543.5	1092.5	1091.9	1087
2	1050.4	1049.4	1039.7	2100.9	2098.8	2079.4
3	1680.7	1680.1	1670.5	3361.5	3358.9	3341
4	1890.8	1888.7	1867.5	3781.7	3777.3	3735
5	2185	2180.1	2143.7	4370.1	4360.3	4278.4
6	3025.4	3015.3	2935.1	6050.8	6030.6	5870.2
7	3067.4	3064	3028.7	6134.8	6127.9	6057.5
8	3571.6	3569.5	3553.3	7143.3	7138.6	7106.5
9	4075.9	4064.9	4048.3	8151.82	8129.3	7982.4
10	4201.9	4185.1	4526.9	8403.9	8370.6	8096.7

Table 4 Effect of thickness ratio (h/b) on the natural frequencies of antisymmetric modes of rectangular plates

Support condition	a/b	m, n	h/b ratio							
			0.005		0.01		0.02			
			Present	[73]	Present	[73]	Present	[73]	[74]	CPT [73]
SSSS	0.5	1,1	1.962277	1.962988	1.962277	1.961786	1.962277	1.956665	1.963495	1.963495
SCSC	1	3,2	22.231423	22.30661	22.231423	22.25712	22.231423	22.06286	22.31424	22.31424
SSSC	2	4,1	32.816831	32.89453	32.816831	32.87303	32.816831	32.87303	32.89686	32.89686
SSSF	0.5	1,4	5.901229	5.898097	5.901229	5.884730	5.901229	5.833354	5.908996	5.908996
SCSF	1	2,1	6.637901	6.610726	6.637901	6.609886	6.637901	6.598192	6.637068	6.637068
SFSF	2	2,3	23.348821	23.29759	23.348821	23.28252	23.348821	23.19873	23.38027	23.38027

30 and 31. The frequency parameter increases with the increase in the aspect ratio r_i/r_o and is found to be maximum for fully clamped end condition in comparison to others.

L-Shaped Plate

The free vibration analysis of L-shaped plate (Fig. 32) under different boundary conditions is performed and the results obtained are presented in Tables 13, 14 which agree well with the existing ones. The minor variation of results can be attributed to the manner in which the boundary condition are imposed in each case. This issue of implementation of the support conditions is well documented in Shojaee et al. [58]. It is observed that the dimensionless natural frequencies of a fully clamped L-shaped plate is more in comparison to a simply supported and completely free one.

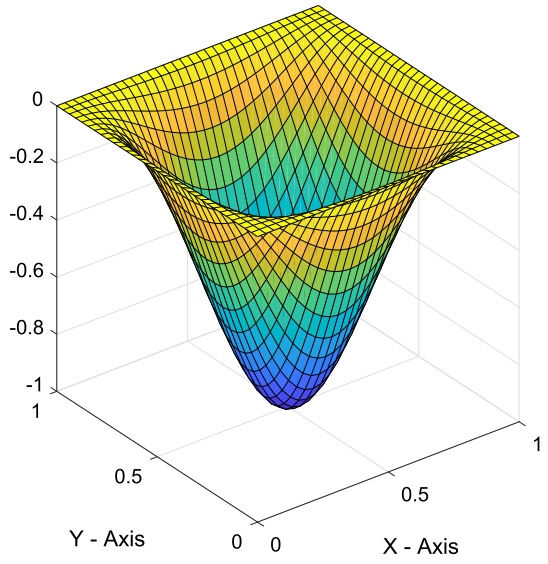

Fig. 5 Mode 1 of rectangular plate having aspect ratio $a/b = 1.0$ for CCCC boundary condition

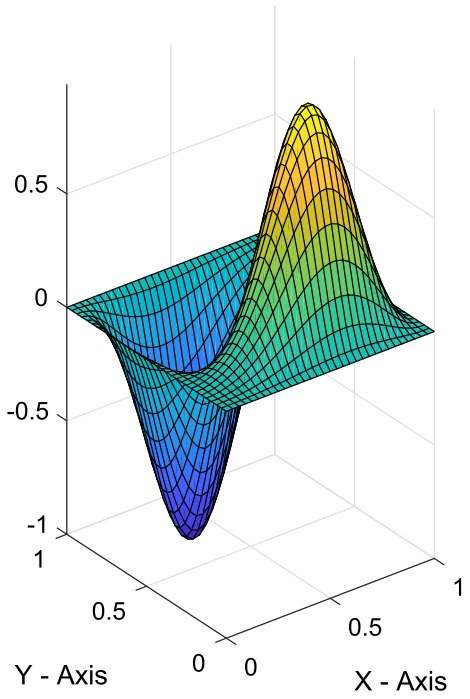

Fig. 7 Mode 3 of rectangular plate having aspect ratio $a/b = 1.0$ for CCCC boundary condition

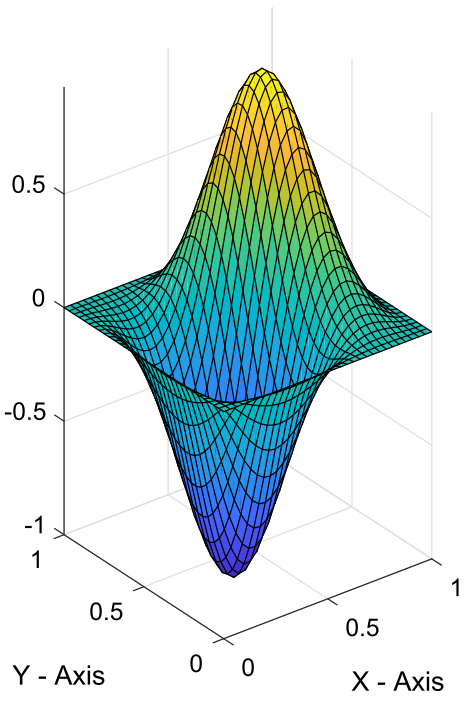

Fig. 6 Mode 2 of rectangular plate having aspect ratio $a/b = 1.0$ for CCCC boundary condition

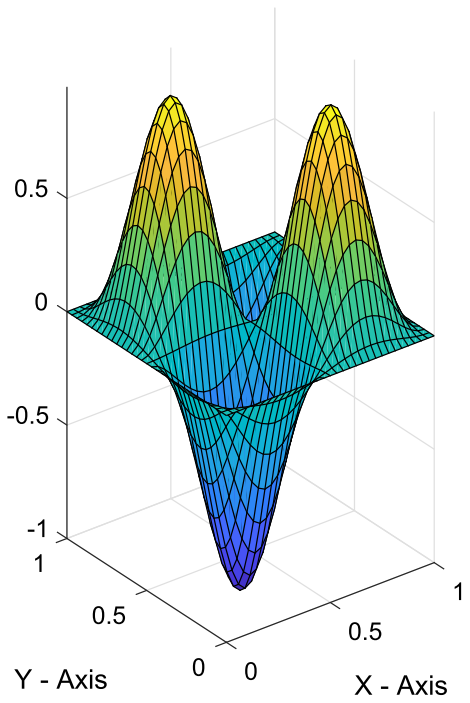

Fig. 8 Mode 4 of rectangular plate having aspect ratio $a/b = 1.0$ for CCCC boundary condition

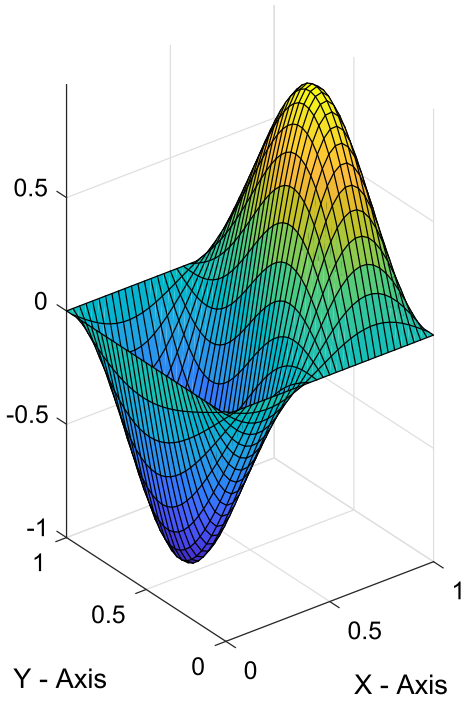

Fig. 9 Mode 1 of rectangular plate having aspect ratio $a/b = 1.0$ for SSSS boundary condition

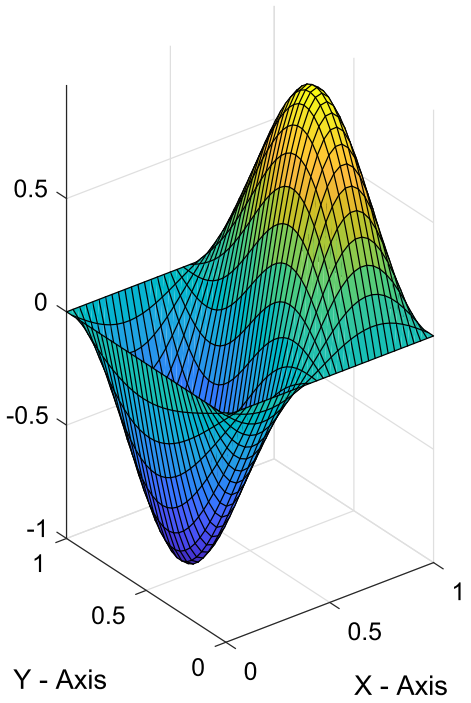

Fig. 10 Mode 2 of rectangular plate having aspect ratio $a/b = 1.0$ for SSSS boundary condition

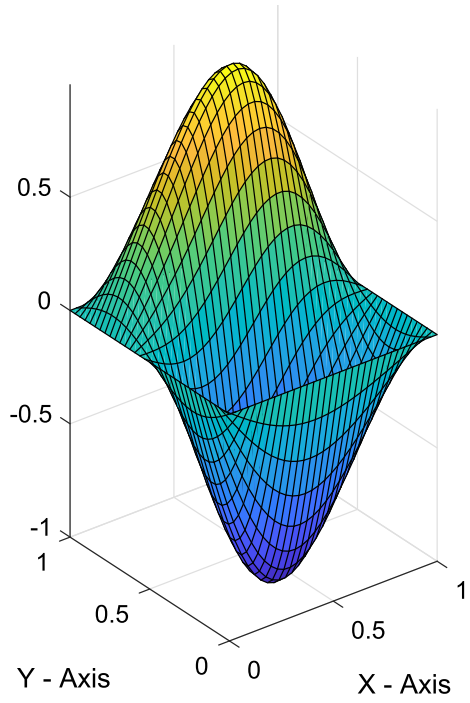

Fig. 11 Mode 3 of rectangular plate having aspect ratio $a/b = 1.0$ for SSSS boundary condition

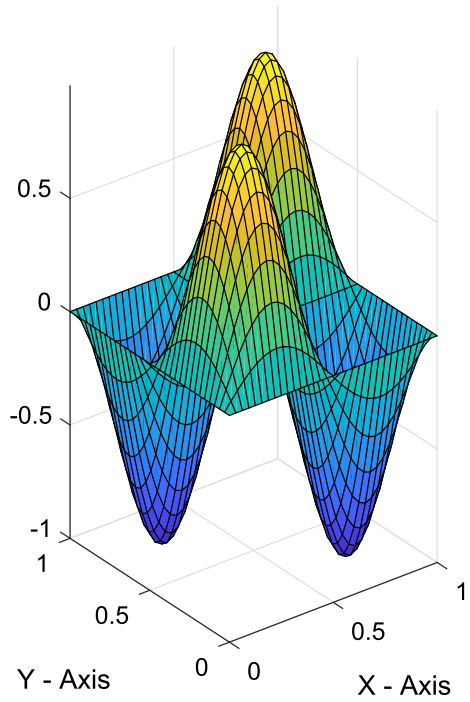

Fig. 12 Mode 4 of rectangular plate having aspect ratio $a/b = 1.0$ for SSSS boundary condition

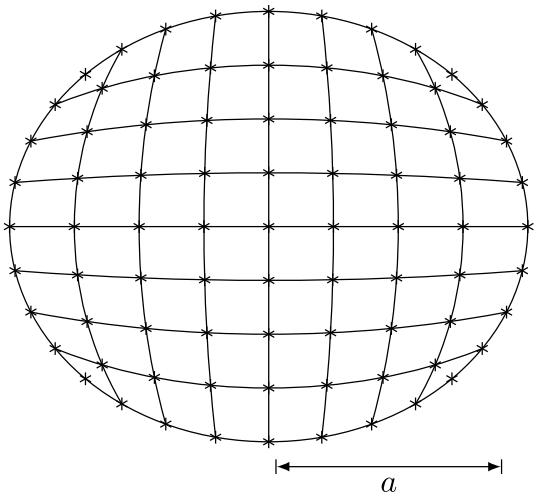

Fig. 13 A typical circular plate with having 8 × 8 mesh

Table 6 Dimensionless natural frequencies $\left(\beta_1 = (\omega^2 a^4 \rho h/D)^{\frac{1}{4}}\right)$ of a fully clamped circular plate

A^*	B^*	D^*	E^*	H^*	G^*
1	3.197	3.1951	3.1962	3.2041	3.1947
2	4.6108	4.6069	4.6109	4.6313	4.6119
3	4.6108	4.6069	4.6109	4.6313	4.6119
4	5.9033	5.8968	5.9059	5.9376	5.9110
5	5.9036	5.8970	5.9059	5.9376	5.9110
6	6.3038	6.2958	6.3064	6.3475	6.3411
7	7.1375	7.1278	7.1442	7.1877	7.2146
8	7.1376	7.1278	7.1442	7.1877	7.2146
9	7.7932	7.7790	7.7987	7.8832	7.8721
10	7.7932	7.7790	7.7987	7.8832	7.8721

A^* mode, B^* present, E^* Hinton [77], D^* Shojaee et al. [58], G^* Cheung et al. [4], H^* Liew et al. [9]

Table 5 Dimensionless natural frequencies $\left(\beta_1 = (\omega^2 a^4 \rho h/D)^{\frac{1}{4}}\right)$ of a completely free circular plate

A^*	B^*	$*D^*$	E^*	
			MKI	EFG
4	2.3147	2.3135	2.2133	2.3375
5	2.3149	2.3135	2.3362	2.3375
6	3.0005	2.9976	2.9776	3.0343
7	3.5264	3.5232	3.5478	3.6007
8	3.5227	3.5232	3.5478	3.6007
9	4.5227	4.5167	4.5084	4.6167
10	4.5227	4.5167	4.5084	4.6167
11	4.6714	4.6652	4.7297	4.8818
12	4.6714	4.6654	4.7684	4.8818
13	5.7846	5.7744	5.9089	6.0586
14	5.7846	5.7744	5.9176	6.0586

A^* mode , B^* present, D^* Shojaee et al. [58], E^* Bui and Nguyen [76]

Table 7 Dimensionless natural frequencies $\left(\beta_1 = (\omega^2 a^4 \rho h/D)^{\frac{1}{4}}\right)$ of a simply supported circular plate

A^*	B^*	D^*	E^*	G^*	
				EFG	SFSM
1	2.2208	2.2208	2.2159	2.2246	2.2197
2	3.7264	3.7252	3.7043	3.7371	3.7256
3	3.7264	3.7252	3.7060	3.7371	3.7256
4	5.0557	5.0541	5.1647	5.1456	5.0537
5	5.0586	5.0541	5.1795	5.1457	5.0537
6	5.4484	5.4431	5.9071	5.9184	5.4626
7	6.3136	6.3082	6.0480	6.4274	6.3482
8	6.314	6.3082	6.4444	6.4274	6.3282
9	6.9576	6.9456	7.4871	7.4705	6.9950
10	6.9603	6.9456	7.4871	7.4705	6.9950

A^* mode, B^* present, D^* Shojaee et al. [58], E^* Bui and Nguyen [76], G^* Cheung et al. [4]

Semi-circular Semi-elliptical Plate

The free vibration analysis of a plate consisting of a semi-circle and semi-ellipse (Fig. 33) is carried out for different boundary conditions and aspect ratios b/a (where a is the radius of the semi-circle and the semi-minor axis of the semi-ellipse and b is the semi-major axis of the semi-ellipse) and the results are presented in Table 15. The boundary conditions are depicted with C—clamped, S—simply supported and F—free end in the anti-clockwise direction starting from the left edge of the plate in the following sequence AB–BD–DE–EA. It is observed that the dimensionless natural frequencies of a fully clamped semi-circular semi-elliptical plate is highest in comparison to other ends. The first four mode shapes of semi-circular semi-elliptical plate having aspect ratio $a/b = 1.125$ under clamped and CSFF boundary conditions are presented in Figs. 34, 35, 36, 37, 38, 39, 40 and 41.

Table 8 Frequency parameters $\lambda = \omega a^2(\rho h/D)^{\frac{1}{2}}$ for skew rhombic plate

A^*	B^*	D^*	1	2	3	4	5	6
H^*	30°	G^*	24.92	52.592	71.726	83.652	122.41	122.67
		E^*	25.0219	52.5501	71.9398	83.5642	122.031	122.558
	45°	G^*	34.985	66.194	99.978	107.47	140.01	168.0
		E^*	35.6320	66.1028	99.9479	108.844	139.403	167.678
	60°	G^*	64.004	104.59	146.93	193.69	208.69	244.57
		E^*	66.3452	104.637	147.839	194.135	213.670	245.783
I^*	30°	G^*	46.029	81.457	105.0	118.79	164.12	165.12
		E^*	45.9824	81.3367	104.849	118.479	163.449	164.744
	45°	G^*	65.515	106.18	147.46	156.84	195.16	228.8
		E^*	65.4204	105.950	146.859	156.569	193.976	228.140
	60°	G^*	121.2	176.52	228.89	286.32	303.41	346.91
		E^*	121.274	176.750	229.394	287.224	303.618	347.786

B^* skew angle θ , D^* method, E^* Barik [6], H^* SSSS, I^* CCCC, A^* support condition, G^* present

Table 9 Frequency parameters $\lambda = \omega a^2(\rho h/D)^{\frac{1}{2}}$ for skew rhombic plate

A^*	B^*	D^*	1	2	3	4	5	6
L^*	15°	G^*	1.0337	1.6699	3.6437	4.2006	5.1348	6.7129
		K^*	1.0334	1.6707	3.6461	4.1994	5.1354	-
	30°	G^*	1.2317	1.7937	3.6474	5.0086	6.2133	6.6335
		K^*	1.2314	1.7960	3.6510	5.0093	6.2220	–
	45°	G^*	1.6627	2.0654	4.0119	6.0416	7.9786	8.2241
		K^*	1.6689	2.0809	4.0185	6.0717	8.0323	–
	60°	G^*	2.5604	2.6872	5.4412	7.3132	10.103	13.68
		K^*	2.6198	2.7716	5.4780	7.4916	10.3010	–
M^*	15°	G^*	3.1076	5.7388	7.5528	9.5059	11.329	13.801
		K^*	3.1107	5.7466	7.5640	9.5336	11.3575	–
	30°	G^*	3.7398	6.5043	9.4063	10.182	13.919	14.392
		K^*	3.7492	6.5167	9.4408	10.2251	13.9867	–
	45°	G^*	5.2965	8.45	12.431	13.843	16.907	19.524
		K^*	5.3457	8.4902	12.5526	14.0132	17.1946	–
	60°	G^*	9.7212	13.8220	18.865	23.761	27.013	29.697
		K^*	10.0306	14.1209	19.6326	25.5291	28.0936	–
N^*	15°	G^*	2.3657	2.7686	4.5391	6.5378	7.1302	8.0125
		K^*	2.3665	2.7710	4.5453	6.5396	7.1366	–
	30°	G^*	2.7769	3.0955	5.0069	7.4906	8.2049	8.6228
		K^*	2.7784	3.1015	5.0246	7.5045	8.2327	–
	45°	G^*	3.6974	3.8569	6.2328	8.781	10.391	11.543
		K^*	3.7121	3.8944	6.2790	8.8629	10.5569	–
	60°	G^*	5.8303	5.8973	9.7416	11.74	14.711	19.52
		K^*	6.0571	6.0758	9.9485	12.3071	15.6104	–

A^* support condition, D^* method, K^* Shojaee et al. [58], G^* present, L^* SFSF, M^* SCSC, N^* CFCF, B^* skew angle θ

Rectangular Plate with Curved Edges

A rectangular plate having curved edges (Fig. 42) is analyzed for different boundary conditions and aspect ratios r_1/r_2 (where r_1 and r_2 are the semi-major and semi-minor axes of the plate respectively) and the results are presented in Table 16. The boundary conditions are depicted with C—clamped, S—simply supported and F—free end in

Table 10 Frequency parameters $\lambda = \omega a^2(\rho h/D)^{\frac{1}{2}}$ for skew rhombic plate

A^*	B^*	D^*	1	2	3	4	5	6
O^*	15°	G^*	0.3631	0.8808	2.2532	2.6676	3.431	5.27
		K^*	0.3632	0.8814	2.2531	2.6686	3.4321	–
	30°	G^*	0.3981	0.9528	2.5641	2.627	4.1885	5.125
		K^*	0.3985	0.9545	2.5652	2.6286	4.1916	–
	45°	G^*	0.4571	1.1367	2.7347	3.1992	5.1345	5.9777
		K^*	0.4579	1.1458	2.7427	3.2118	5.1444	–
	60°	G^*	0.5347	1.6199	3.0975	4.6171	5.9878	8.1663
		K^*	0.5394	1.6433	3.1657	4.6804	6.0773	–

A^* support condition, B^* skew angle θ, D^* method, G^* present, K^* Shojaee et al. [58], O^* CFFF

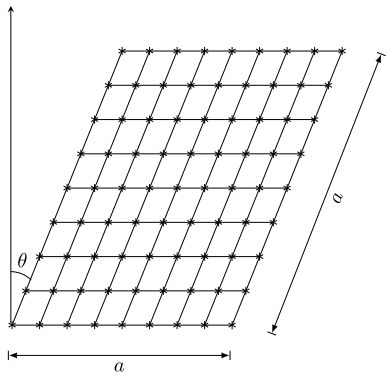

Fig. 14 A typical skew rhombic plate having 8 × 8 mesh

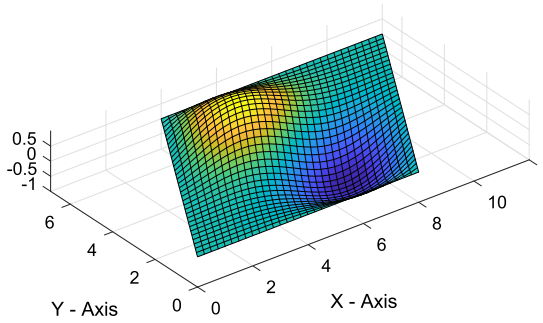

Fig. 17 Mode 3 of skew plate having aspect ratio $a/b = 1.0$ and skew angle $\theta = 30°$ under SSSS boundary condition

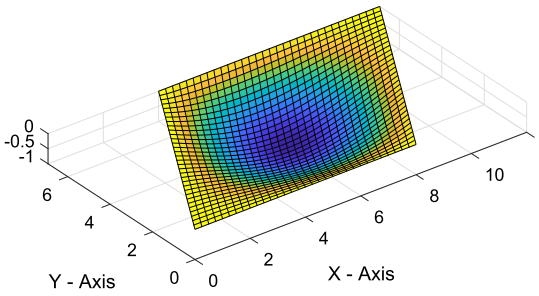

Fig. 15 Mode 1 of skew plate having aspect ratio $a/b = 1.0$ and skew angle $\theta = 30°$ under SSSS boundary condition

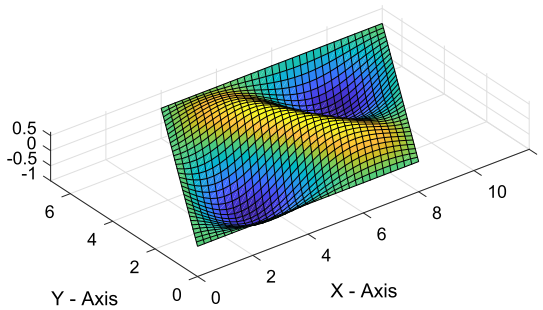

Fig. 18 Mode 4 of skew plate having aspect ratio $a/b = 1.0$ and skew angle $\theta = 30°$ under SSSS boundary condition

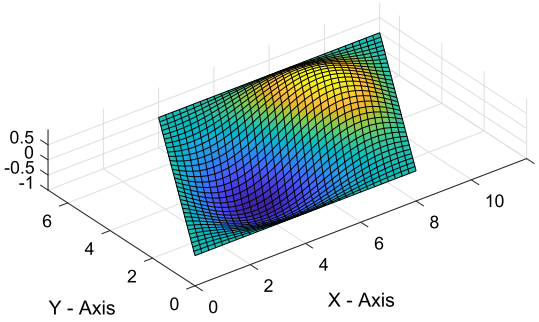

Fig. 16 Mode 2 of skew plate having aspect ratio $a/b = 1.0$ and skew angle $\theta = 30°$ under SSSS boundary condition

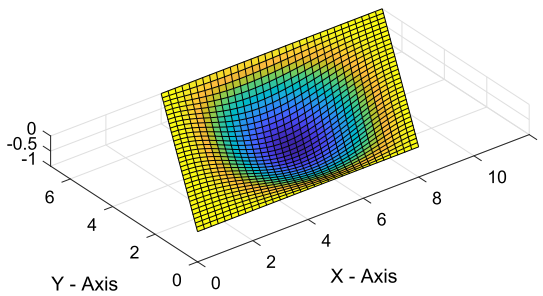

Fig. 19 Mode 1 of skew plate having aspect ratio $a/b = 1.0$ and skew angle $\theta = 30°$ under SCSC boundary condition

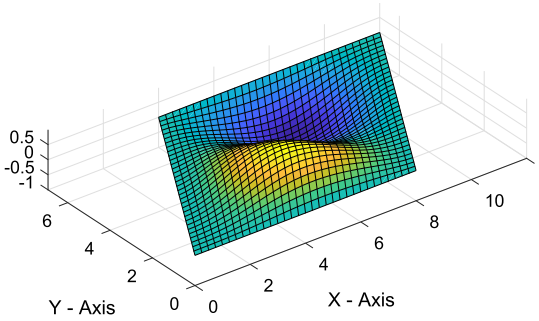

Fig. 20 Mode 2 of skew plate having aspect ratio $a/b = 1.0$ and skew angle $\theta = 30°$ under SCSC boundary condition

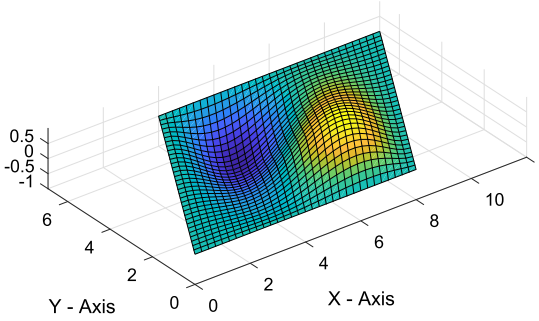

Fig. 21 Mode 3 of skew plate having aspect ratio $a/b = 1.0$ and skew angle $\theta = 30°$ under SCSC boundary condition

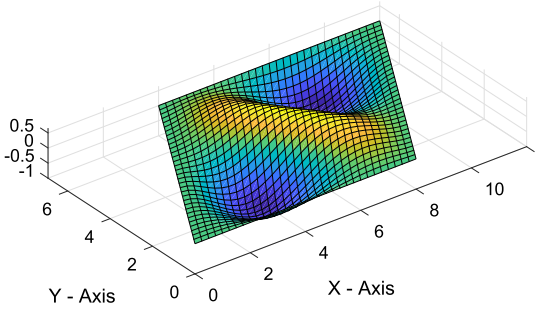

Fig. 22 Mode 4 of skew plate having aspect ratio $a/b = 1.0$ and skew angle $\theta = 30°$ under SCSC boundary condition

the anti-clockwise direction starting from the left edge of the plate in the following sequence AB–BD–DE–EA. It is observed that the natural frequency for a rectangular plate with curved edges increases with the increase in the aspect ratios r_1/r_2 and is highest for fully clamped edge condition.

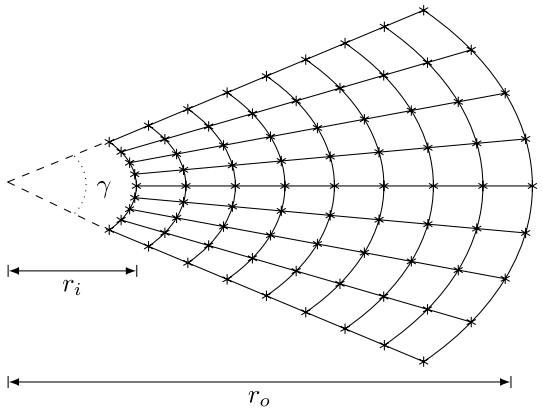

Fig. 23 A typical annular plate with 8×8 mesh

First four mode shapes of the plate having aspect ratio $r_1/r_2 = 1.5$ under clamped and CCSS boundary conditions are shown in Figs. 43, 44, 45, 46, 47, 48, 49 and 50.

Dome-Shaped Plate

A typical plate resembling the shape of a dome is considered by taking one of the edges straight and its opposite edge as the top of a dome (Fig. 51). The free vibration analysis of this dome-shaped plate is carried out for different boundary conditions and aspect ratio r_1/r_2 where r_1 is half the length of the straight edge and r_2 is the semi-minor axis of the dome. The results obtained are presented in Table 17. The boundary conditions are depicted with C—clamped, S—simply supported and F—free end in the anti-clockwise direction starting from the left edge of the plate in the following sequence EA–AB–BD–DE. It is observed that the natural frequency for a dome-shaped plate increases with the increase in the aspect ratios r_1/r_2 and is highest for fully clamped edge condition. First four mode shapes of the plate having aspect ratio $r_1/r_2 = 1.5$ under different clamped and CCCS boundary conditions are shown in Figs. 52, 53, 54, 55, 56, 57, 58 and 59. The dimensionless natural frequency increases with the increase in aspect ratio and was found to be maximum for all edges clamped condition.

Rectangular Plate with One-Side Curved Edge

A rectangular plate with one side being curved is analyzed by considering the rectangular portion as patch-1 (32×32 mesh) and the remaining portion as patch-2 (32×32 mesh)

Table 11 Frequency parameters $\lambda = \omega a^2(\rho h/D)^{\frac{1}{2}}$ for clamped annular sector plate

r_i/r_o	B^*	1	2	3	4	5
0.25	M^*	52.61	87.82	123.51	136.61	167.62
	I^*	52.01	87.60	121.18	136.01	166.65
	H^*	52.58	87.72	123.43	136.38	167.21

B^* method, H^* Barik [7] , M^* present, I^* Mukhopadhyay [3]

Table 12 Frequency parameters $\lambda = \omega a^2(\rho h/D)^{\frac{1}{2}}$ for annular sector plate

A^*	r_i/r_o	B^*	1	2	3	4	5
D^*	0.25	M^*	32.21	64.15	88.53	107.48	133.47
		I^*	32.18	64.41	88.35	107.91	133.91
		H^*	32.21	64.11	88.50	107.19	133.22
	0.5	M^*	48.70	72.868	111.15	161.68	167.58
		I^*	48.74	73.34	111.82	166.90	193.20
		H^*	48.69	72.81	111.03	161.22	167.49
E^*	0.25	M^*	28.401	56.542	85.093	97.394	124.01
		I^*	28.345	56.719	84.687	97.653	123.949
		H^*	28.407	56.507	85.077	97.225	123.669
	0.5	M^*	47.188	68.05	102.91	150.26	166.64
		I^*	47.142	68.264	103.224	150.747	165.734
		H^*	47.182	67.986	102.732	149.938	166.556

A^* support condition, B^* method, D^* CSSS, E^* SSSS, H^* Barik [7], M^* present, I^* Mukhopadhyay [3], G^* SSSS

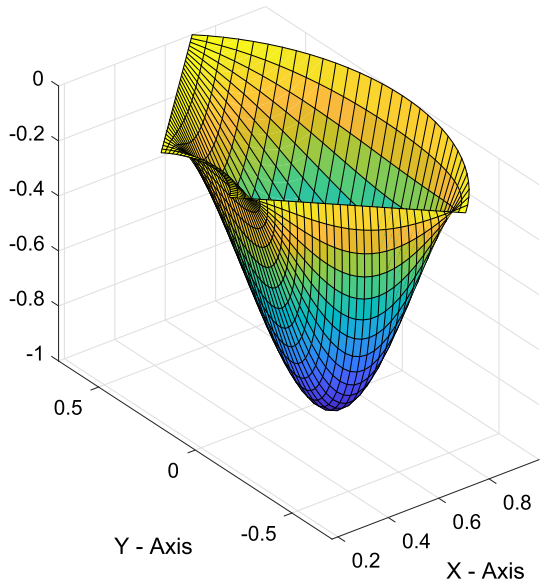

Fig. 24 Mode 1 of annular sector plate having $r_i/r_o = 0.25$ under CSSS boundary condition

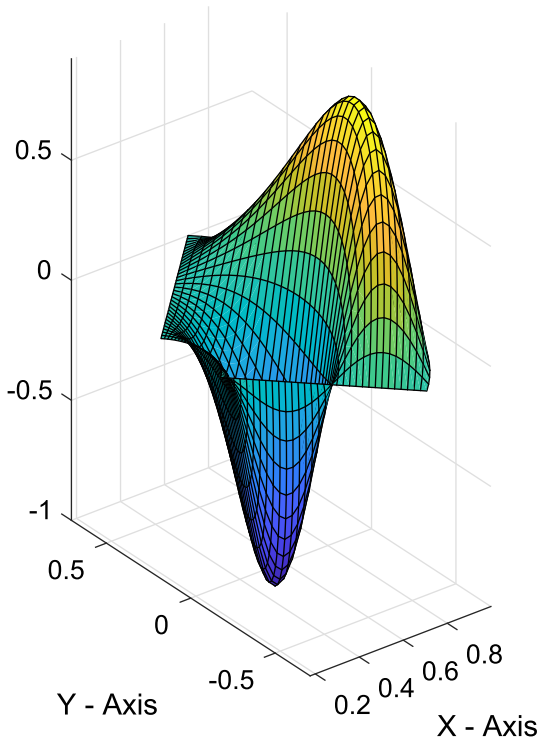

Fig. 25 Mode 2 of annular sector plate having $r_i/r_o = 0.25$ under CSSS boundary condition

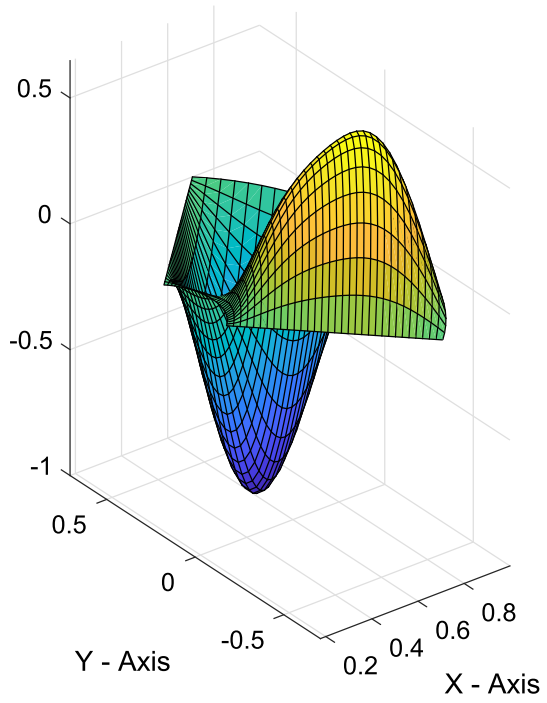

Fig. 26 Mode 3 of annular sector plate having $r_i/r_o = 0.25$ under CSSS boundary condition

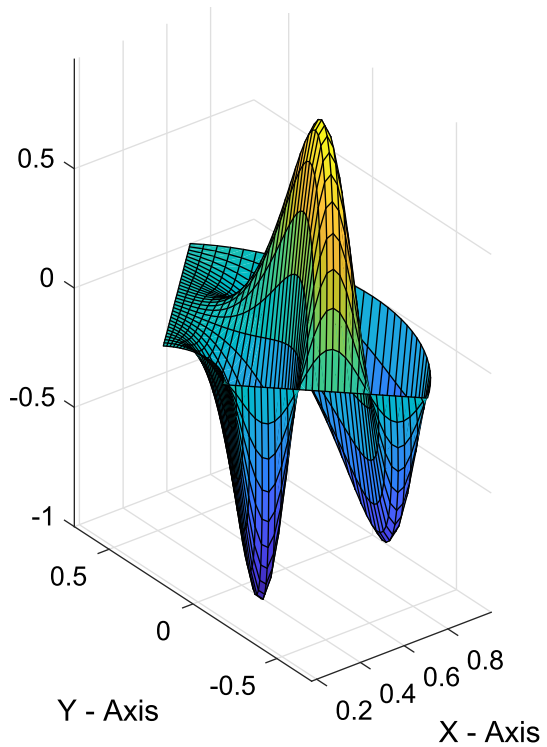

Fig. 27 Mode 4 of annular sector plate having $r_i/r_o = 0.25$ under CSSS boundary condition

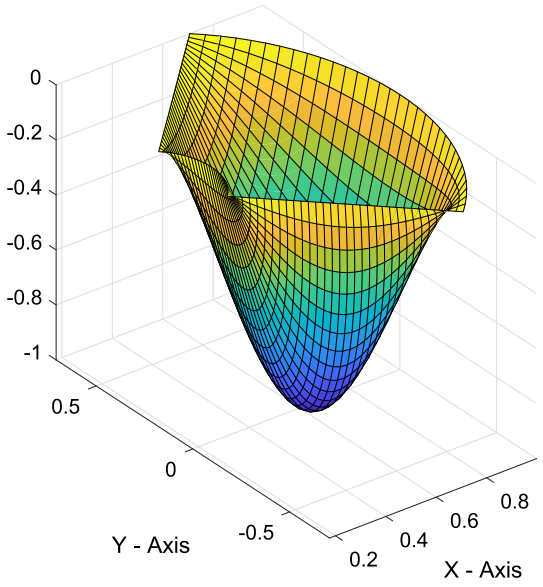

Fig. 28 Mode 1 of annular sector plate having $r_i/r_o = 0.25$ under SSSS boundary condition

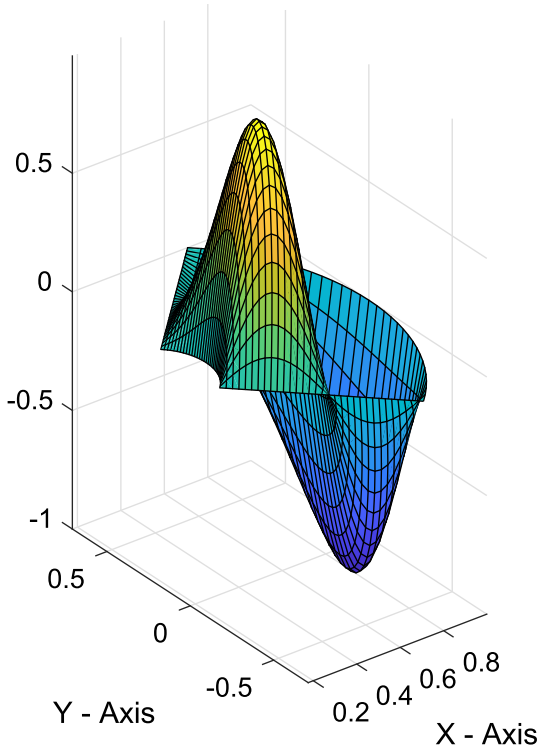

Fig. 29 Mode 2 of annular sector plate having $r_i/r_o = 0.25$ under SSSS boundary condition

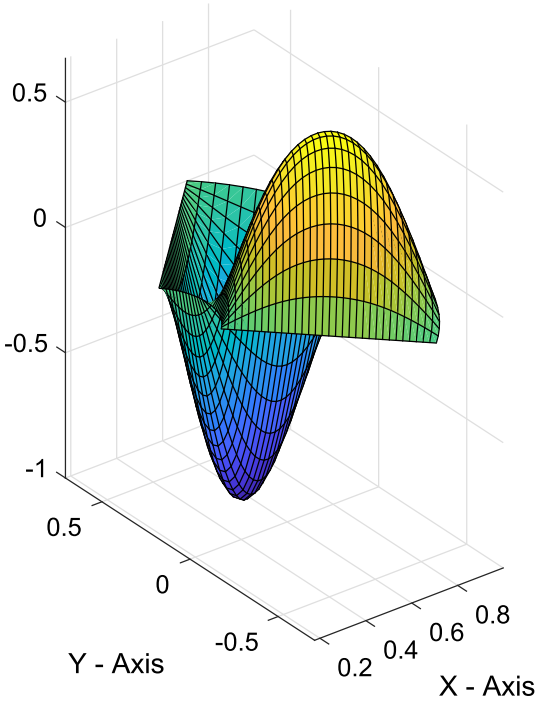

Fig. 30 Mode 3 of annular sector plate having $r_i/r_o = 0.25$ under SSSS boundary condition

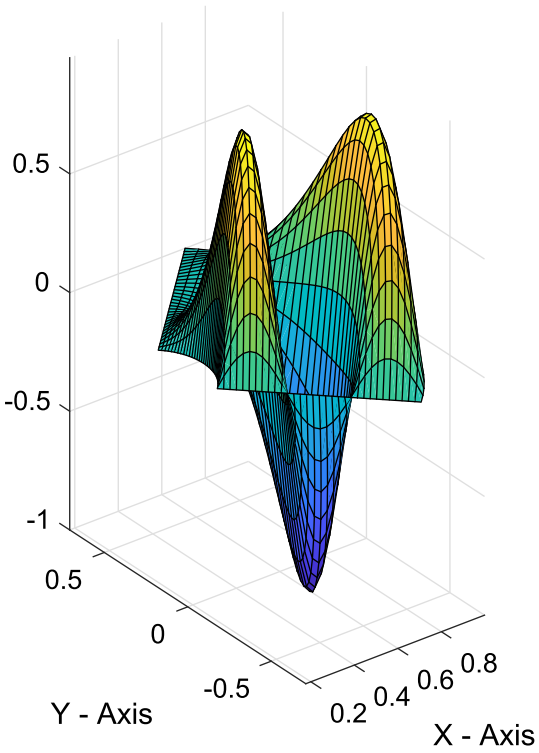

Fig. 31 Mode 4 of annular sector plate having $r_i/r_o = 0.25$ under SSSS boundary condition

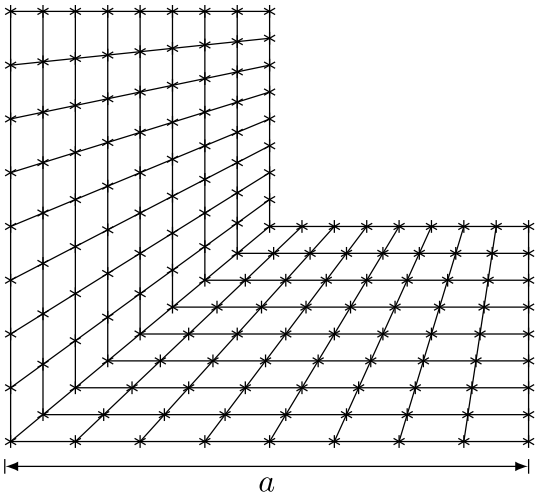

Fig. 32 A typical L-shaped plate with 8 × 8 mesh

Table 13 Dimensionless natural frequencies $\beta_1 = (\omega^2 a^4 \rho h/D)^{\frac{1}{4}}$ of a completely free L-shaped plate

P^*	M^*	N^*	O^*	
			MKI	EFG
4	3.4342	4.0267	3.9694	3.9796
5	4.1301	4.1354	4.1284	4.1790
6	5.8074	5.3302	5.2122	5.2253
7	5.8876	5.8005	5.7019	5.8294
8	7.7005	7.7589	7.6153	7.7726
9	7.7573	7.8008	7.7838	7.8009
10	8.9589	8.2518	8.1233	8.0450
11	9.5363	9.5159	9.2627	9.5221
12	9.8932	9.8811	9.7246	9.8178
13	9.9772	9.9610	9.9391	10.0634
14	11.1	10.9044	10.3906	10.8019
15	11.222	11.2379	11.0938	11.2012

N^* Shojaee et al. [58], P^* mode, M^* present, O^* Bui et al. [78]

under different boundary conditions and aspect ratios *a*/*b* (*a*—length of the rectangular portion, *b*—breadth of the rectangular portion). The nodes of the rectangular portion (patch-1) are represented with asterisk and the remaining portion (patch-2) with circular markers respectively. The results obtained are presented in Table 18. A typical rectangular plate with one-side curved edge consisting of a rectangular portion as patch-1 (4 × 4mesh) and the remaining as

Table 14 Dimensionless natural frequencies $\beta_1 = (\omega^2 a^4 \rho h/D)^{\frac{1}{4}}$ of a L-shaped plate

P^*	A^*	M^*	N^*	O^*		A^*	M^*	N^*
				MKI	EFG			
1	Simply supported	6.9113	6.7498	6.8204	6.7649	Clamped	9.258	9.0559
2		7.4543	7.8268	7.9560	8.0319		9.7297	10.2628
3		8.9911	8.8766	8.4489	8.8821		11.057	11.0427
4		10.409	10.8610	10.4509	10.8853		12.29	12.7108
5		11.582	11.5428	11.1064	11.5584		13.681	13.5290
6		12.158	13.0360	13.2219	13.0156		14.443	15.2262
7		13.097	13.4206	13.3820	13.7309		15.525	15.6192
8		13.572	14.0258	13.9620	14.0279		15.846	16.3538
9		14.358	14.0280	14.0655	14.0442		16.599	16.4143
10		14.885	15.1483	15.2255	15.1630		17.013	17.4016

N^* Shojaee et al. [58], P^* mode, A^* end condition, M^* present, O^* Bui et al. [78]

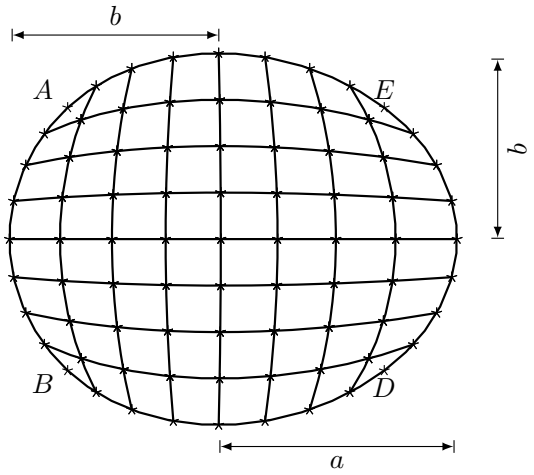

Fig. 33 A typical semi-circular semi-elliptical plate with 8×8 mesh

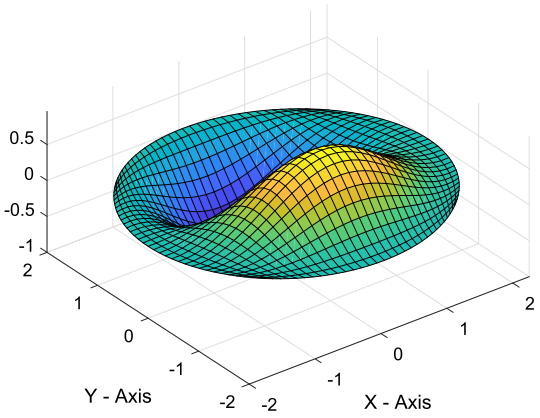

Fig. 35 Mode 2 of semi-circular semi-elliptical plates having aspect ratio $a/b = 1.125$ under CCCC boundary condition

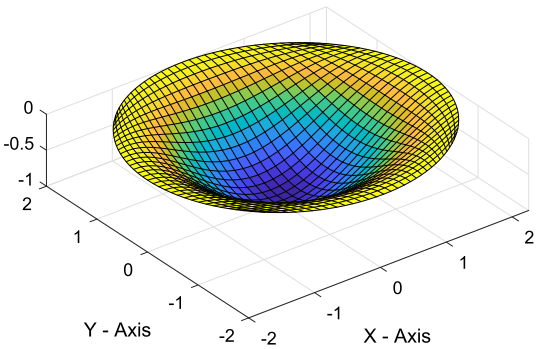

Fig. 34 Mode 1 of semi-circular semi-elliptical plates having aspect ratio $a/b = 1.125$ under CCCC boundary condition

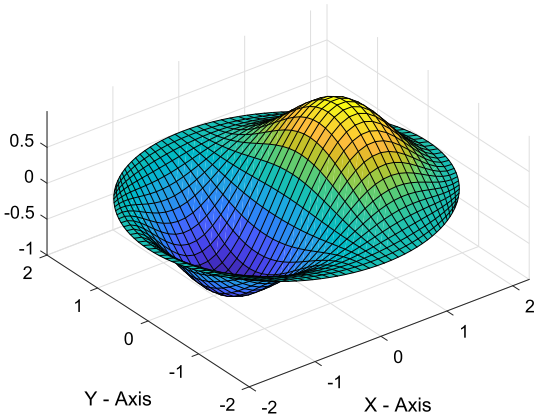

Fig. 36 Mode 3 of semi-circular semi-elliptical plates having aspect ratio $a/b = 1.125$ under CCCC boundary condition

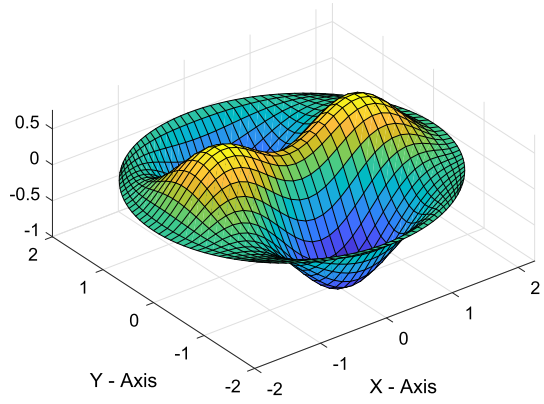

Fig. 37 Mode 4 of semi-circular semi-elliptical plates having aspect ratio $a/b = 1.125$ under CCCC boundary condition

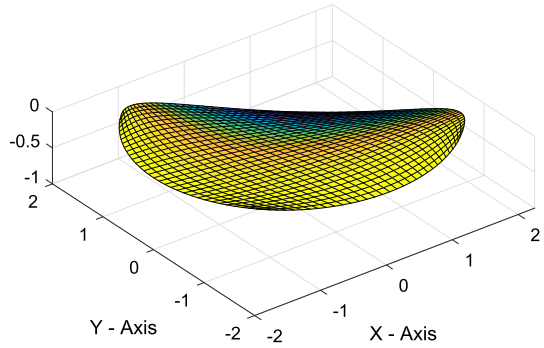

Fig. 38 Mode 1 of semi-circular semi-elliptical plates having aspect ratio $a/b = 1.125$ under CSFF boundary condition

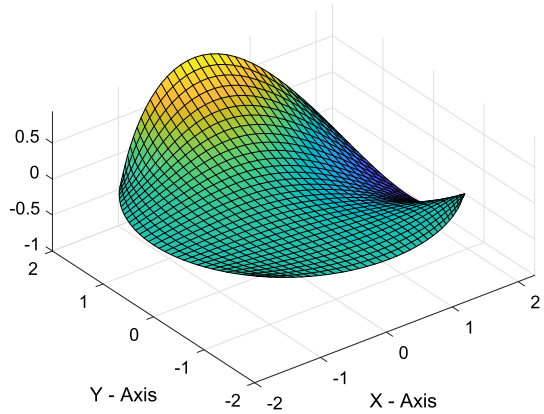

Fig. 39 Mode 2 of semi-circular semi-elliptical plates having aspect ratio $a/b = 1.125$ under CSFF boundary condition

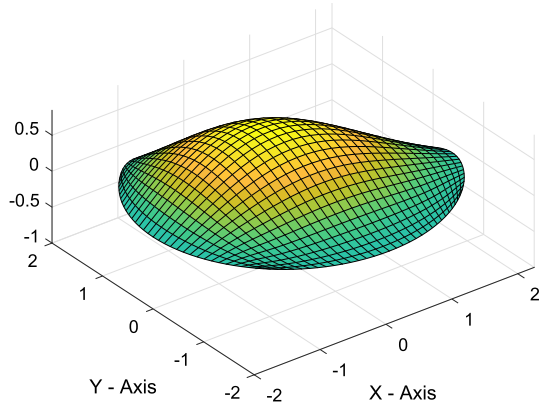

Fig. 40 Mode 3 of semi-circular semi-elliptical plates having aspect ratio $a/b = 1.125$ under CSFF boundary condition

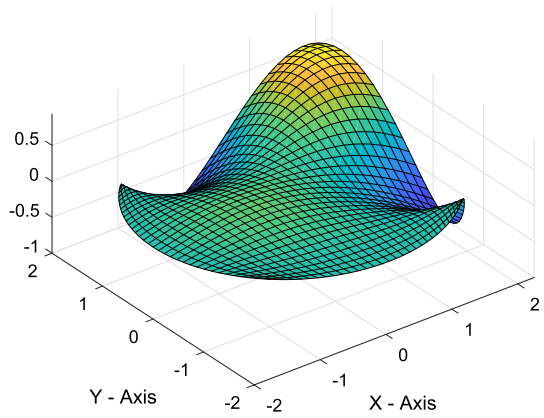

Fig. 41 Mode 4 of semi-circular semi-elliptical plates having aspect ratio $a/b = 1.125$ under CSFF boundary condition

patch-2 (4×4 mesh) is shown in Fig. 60. It is observed that the natural frequency for a rectangular plate with one-side curved edge increases with the increase in the aspect ratios a/b and is highest for fully clamped edge condition.

Conclusions

In the present formulation, NURBS basis functions are used to represent the exact shape of the arbitrary thin plates. In contrast to the isogeometric analysis, the use of classical finite-element basis functions as field variables helps in

Table 15 Dimensionless natural frequencies $\beta_1 = \omega^2 b^2 (\rho h/D)^{\frac{1}{2}}$ of semi-circular semi-elliptical plate

A^*	b/a	1	2	3	4	5	6
B^*	1.125	5.8944	16.009	17.141	30.14	30.502	35.814
	1.25	6.9351	18.15	20.719	34.283	35.745	42.984
D^*	1.125	12.2189	24.619	26.162	41.063	41.598	47.963
	1.25	14.359	28.047	31.55	46.808	48.794	57.591
E^*	1.125	8.6824	12.164	22.316	22.966	30.694	38.841
	1.25	9.7251	14.08	25.671	26.856	34.674	45.576
G^*	1.125	1.2519	3.6539	7.2739	11.476	12.997	19.439
	1.25	1.3794	4.2165	8.0403	13.801	14.777	21.608
H^*	1.125	2.5488	8.2121	9.3186	17.326	20.947	22.649
	1.25	2.9102	9.3931	10.883	19.836	24.567	26.262
I^*	1.125	2.8922	8.5393	11.181	17.856	23.068	25.468
	1.25	3.3743	9.7046	13.326	20.422	26.295	30.766
L^*	1.125	8.9319	20.076	21.511	35.501	35.804	41.439
	1.25	10.521	22.764	25.991	40.347	41.904	49.789

A^*support condition , B^* SSSS, D^* CCCC, E^* CFCS, G^* CFFF, H^* CSFF, I^* CCFF, L^* CCSS

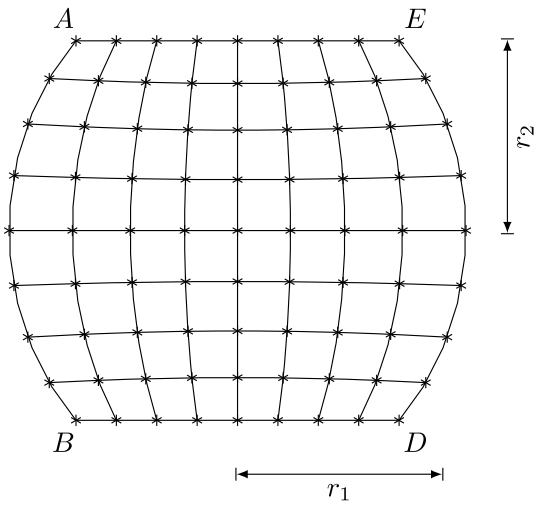

Fig. 42 A typical rectangular plate with curved edges having 8×8 mesh

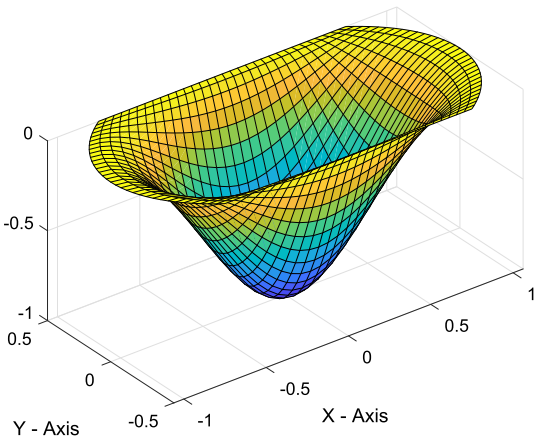

Fig. 43 Mode 1 of rectangular plate with curved edges having aspect ratio $r_1/r_2 = 1.5$ under CCCC boundary condition

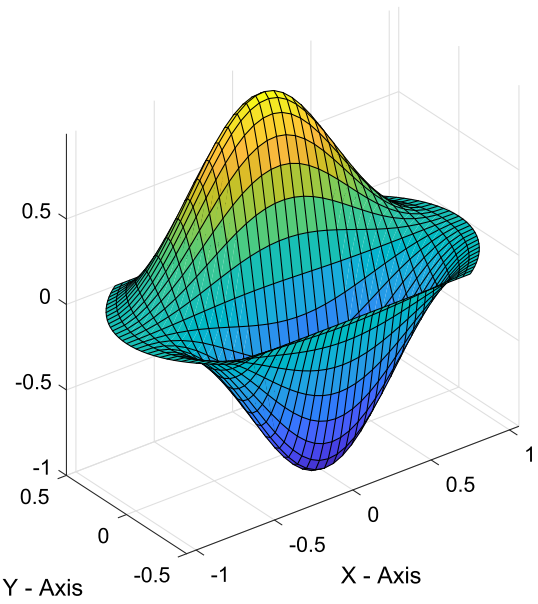

Fig. 44 Mode 2 of rectangular plate with curved edges having aspect ratio $r_1/r_2 = 1.5$ under CCCC boundary condition

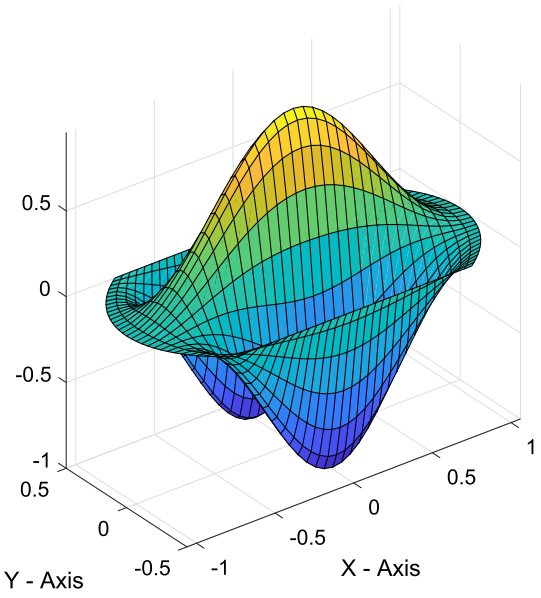

Fig. 45 Mode 3 of rectangular plate with curved edges having aspect ratio $r_1/r_2 = 1.5$ under CCCC boundary condition

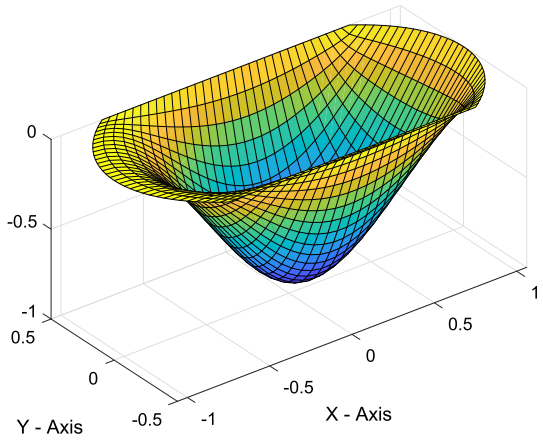

Fig. 47 Mode 1 of rectangular plate with curved edges having aspect ratio $r_1/r_2 = 1.5$ under CCSS boundary condition

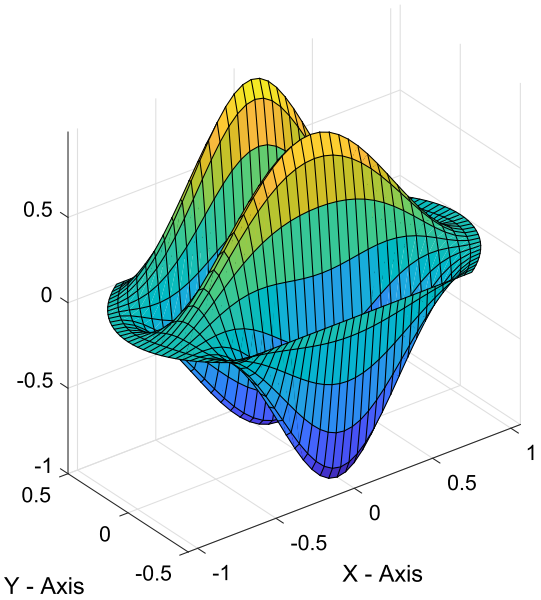

Fig. 46 Mode 4 of rectangular plate with curved edges having aspect ratio $r_1/r_2 = 1.5$ under CCCC boundary condition

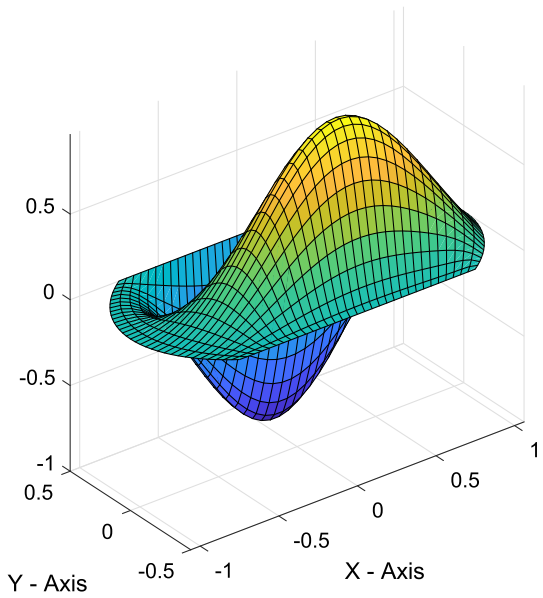

Fig. 48 Mode 2 of rectangular plate with curved edges having aspect ratio $r_1/r_2 = 1.5$ under CCSS boundary condition

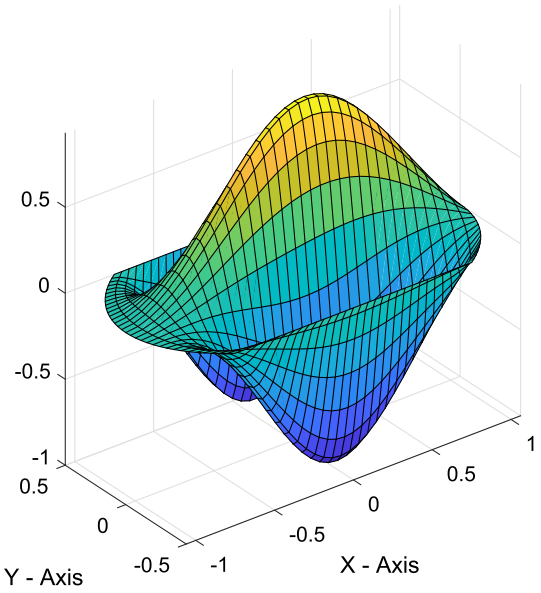

Fig. 49 Mode 3 of rectangular plate with curved edges having aspect ratio $r_1/r_2 = 1.5$ under CCSS boundary condition

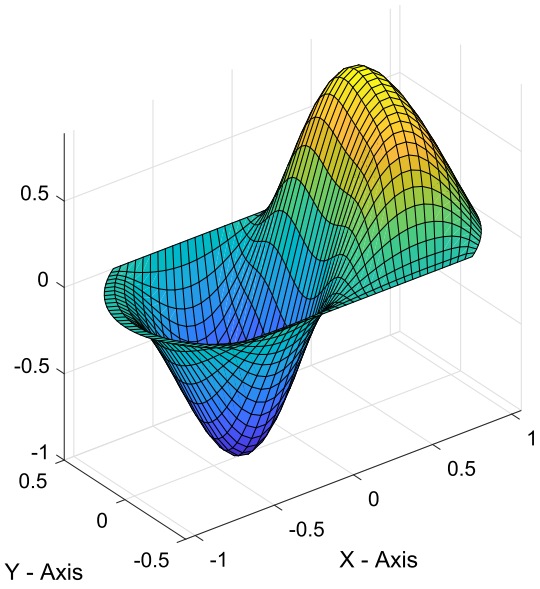

Fig. 50 Mode 4 of rectangular plate with curved edges having aspect ratio $r_1/r_2 = 1.5$ under CCSS boundary condition

Table 16 Dimensionless natural frequencies $\beta_1 = \omega^2 r_1^2(\rho h/D)^{\frac{1}{2}}$ of rectangular plate with curved edges

A^*	r_1/r_2	1	2	3	4	5	6	7	8
B^*	1.0	14.134	23.315	33.887	38.459	43.245	58.743	58.994	63.533
	1.5	27.55	35.421	49.442	69.429	72.169	80.743	94.773	95.484
	2.0	46.908	53.968	66.89	85.987	110.93	126.04	134.28	141.19
D^*	1.0	7.3318	15.175	22.634	28.422	31.421	46.045	46.447	47.485
	1.5	13.523	21.305	34.669	47.434	53.288	56.504	71.594	76.741
	2.0	22.305	30.252	43.753	62.621	82.123	86.511	91.575	107.21
E^*	1.0	10.429	19.081	27.909	33.375	37.037	52.247	52.556	55.269
	1.5	19.8	27.869	41.773	59.09	60.948	68.214	81.928	86.859
	2.0	33.22	40.918	54.51	73.79	97.995	103.07	111.46	126.68
G^*	1.0	2.8495	8.3219	11.976	18.674	20.857	28.712	34.411	36.12
	1.5	4.8798	10.859	20.595	27.786	31.08	43.456	43.944	59.028
	2.0	7.6477	13.855	24.822	38.949	46.722	55.639	59.254	75.281
H^*	1.0	1.6442	6.492	8.8147	15.984	16.653	24.873	29.506	30.196
	1.5	2.4926	8.5386	16.328	21.616	25.11	36.108	39.161	52.153
	2.0	3.2803	10.624	20.936	32.211	34.291	46.204	49.297	64.614
I^*	1.0	1.0944	3.6698	6.7572	12.843	13.083	19.451	23.165	26.049
	1.5	1.1367	5.1211	7.0296	16.988	18.711	29.228	32.929	33.365
	2.0	1.1668	6.5901	7.2224	19.772	21.19	37.187	39.442	48.513
L^*	1.0	5.0872	12.975	13.883	24.908	26.973	29.987	40.091	42.02
	1.5	7.4109	17.519	22.027	33.046	35.978	52.311	54.648	62.043
	2.0	9.6324	22.004	32.615	42.074	46.534	63.925	68.056	88.887
M^*	1.0	8.3939	17.95	23.328	32.686	33.707	48.022	50.102	51.567
	1.5	14.422	24.086	39.341	47.996	58.558	59.562	75.612	84.279
	2.0	23.108	32.987	48.762	69.767	82.619	93.463	95.397	111.13

A^* support condition, B^* CCCC, D^* SSSS, E^* CCSS, G^* CCFF, H^* SSFF, I^* CFFF, L^* SSSF, M^* CSSS

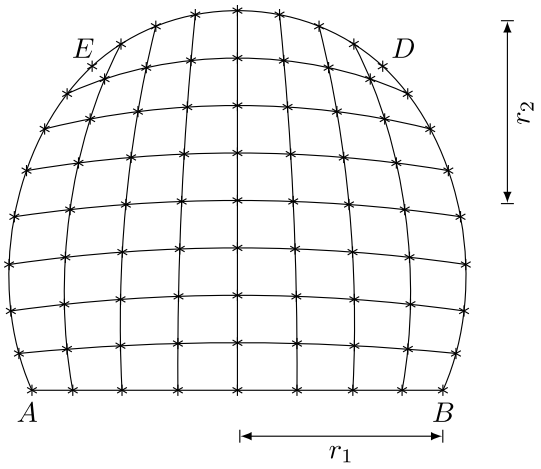

Fig. 51 A typical dome-shaped plate having 8×8 mesh

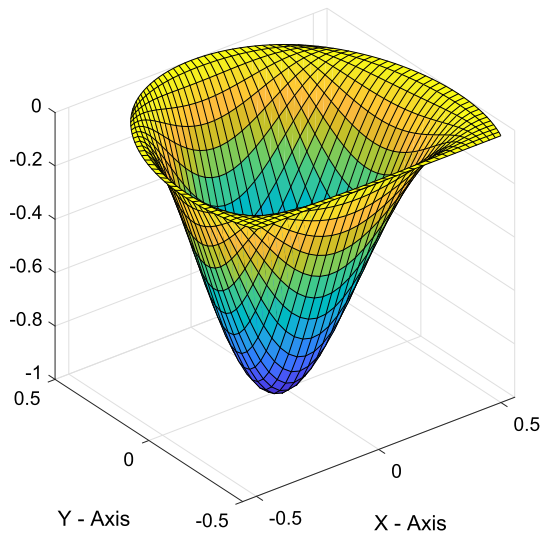

Fig. 52 Mode 1 of a plate in the shape of a dome having aspect ratio $r_1/r_2 = 1.5$ under CCCC boundary condition

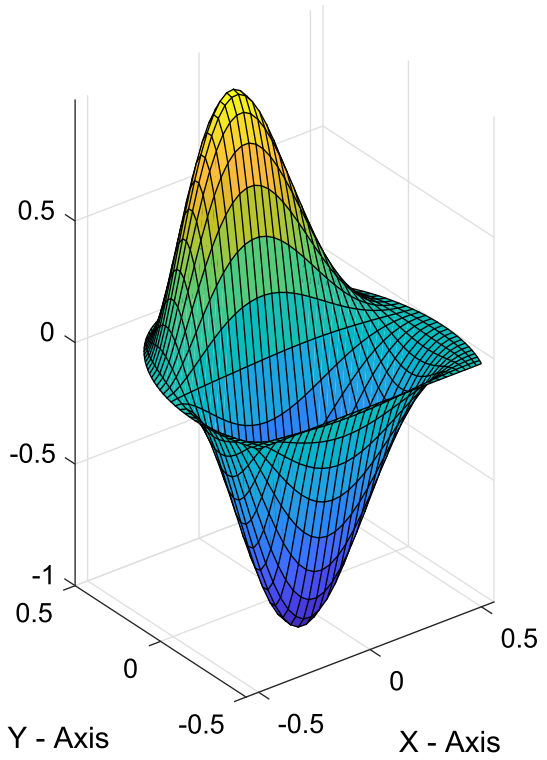

Fig. 53 Mode 2 of a plate in the shape of a dome having aspect ratio $r_1/r_2 = 1.5$ under CCCC boundary condition

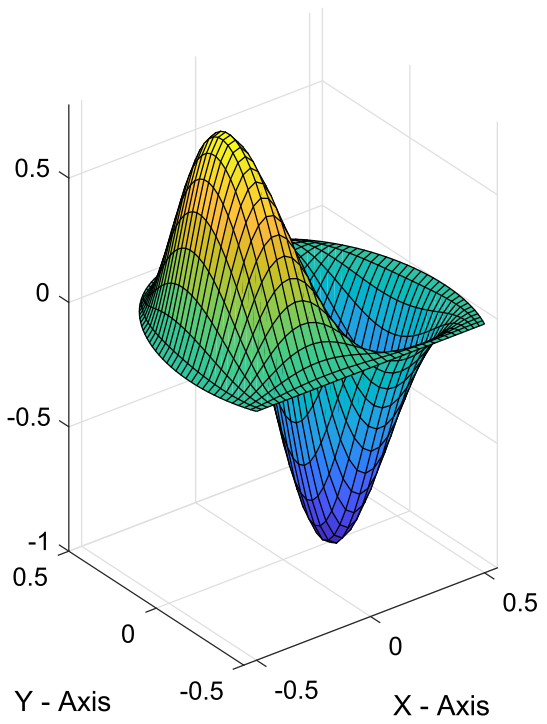

Fig. 54 Mode 3 of a plate in the shape of a dome having aspect ratio $r_1/r_2 = 1.5$ under CCCC boundary condition

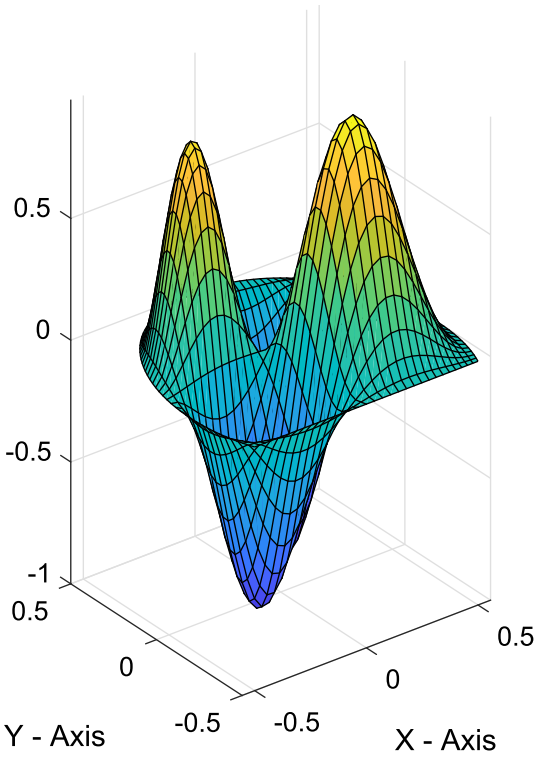

Fig. 55 Mode 4 of a plate in the shape of a dome having aspect ratio $r_1/r_2 = 1.5$ under CCCC boundary condition

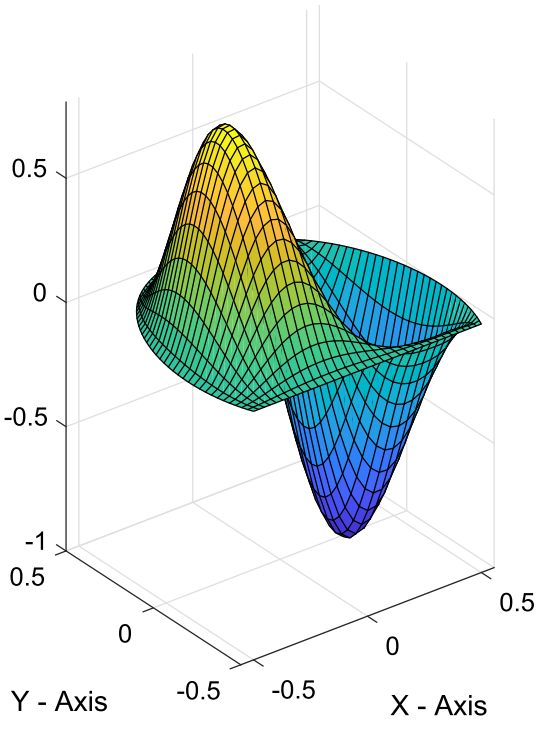

Fig. 57 Mode 2 of a plate in the shape of a dome having aspect ratio $r_1/r_2 = 1.5$ under CCCS boundary condition

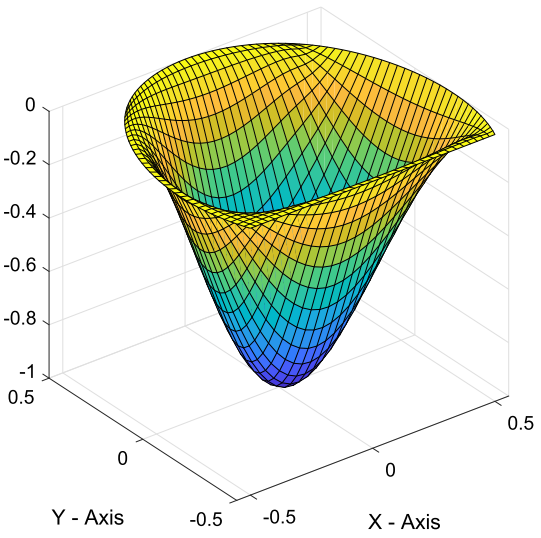

Fig. 56 Mode 1 of a plate in the shape of a dome having aspect ratio $r_1/r_2 = 1.5$ under CCCS boundary condition

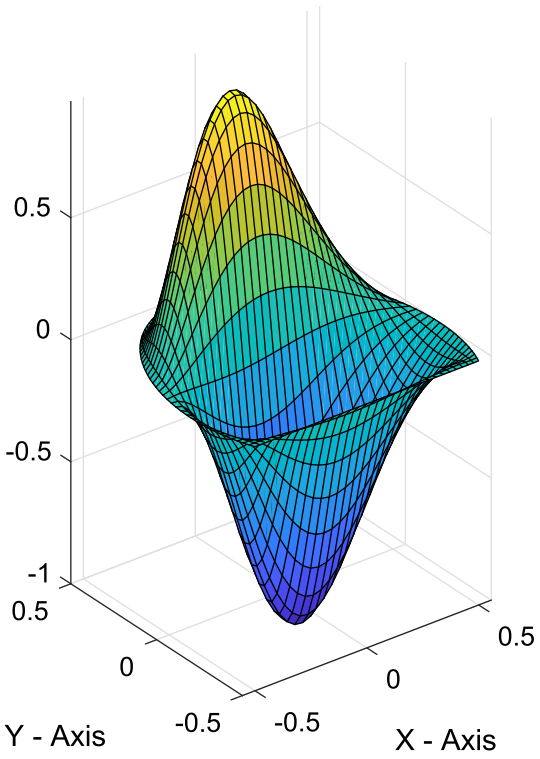

Fig. 58 Mode 3 of a plate in the shape of a dome having aspect ratio $r_1/r_2 = 1.5$ under CCCS boundary condition

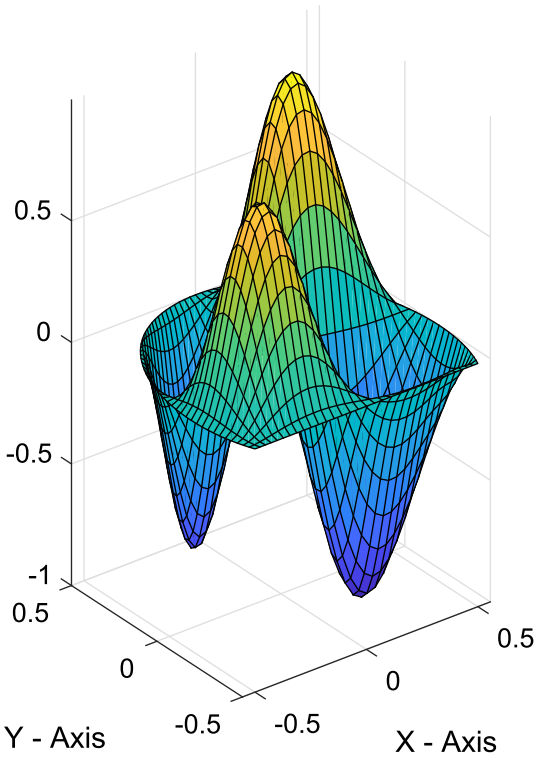

Fig. 59 Mode 4 of a plate in the shape of a dome having aspect ratio $r_1/r_2 = 1.5$ under CCCS boundary condition

imposing the boundary conditions easily which is the main drawback of isogeometric analysis. Further, the knot refinement technique of the NURBS basis function takes care of the mesh generation. The free vibration analysis of arbitrary-shaped plates are carried out and the results obtained are found to be well in agreement with the published ones. To showcase the robustness of NAFEM, some complicated shaped plates (semi-circular semi-elliptical, rectangular plate with curved edges, dome-shaped plate, and L-shaped plate) have been considered for the free vibration analysis and the new results are presented. Further, a rectangular plate with one side being curved is analyzed by considering the rectangular portion as patch-1 and the remaining portion as patch-2 thereby showing the capability of NAFEM to analyze complex geometries by splitting them into more amenable patches which can be dealt with ease.

Table 17 Dimensionless natural frequencies $\beta_1 = \omega^2 r_1^2 (\rho h/D)^{\frac{1}{2}}$ of a dome-shaped plate

A^*	r_1/r_2	1	2	3	4	5	6	7	8
B^*	1.0	9.1039	17.639	19.373	29.21	30.301	34.332	43.842	44.664
	1.5	15.899	24.357	35.576	40.616	47.75	55.82	61.401	74.044
	2.0	25.914	34.621	46.604	61.915	67.627	80.227	81.078	97.924
D^*	1.0	4.6349	11.605	12.793	21.312	22.464	25.554	34.247	34.844
	1.5	7.8681	15.206	24.419	27.949	34.561	42.717	46.682	56.276
	2.0	12.528	20.342	31.379	44.646	45.44	57.43	61.991	73.976
E^*	1.0	6.8313	14.875	15.841	25.378	26.774	29.599	39.263	40.263
	1.5	11.641	20.158	30.208	34.412	40.945	50.352	54.313	64.8
	2.0	18.655	27.71	40.071	54.416	55.802	69.066	71.775	87.618
G^*	1.0	2.2746	6.4523	8.5505	12.995	17.583	18.405	22.15	28.586
	1.5	3.7276	9.3549	15.14	19.229	23.879	31.667	36.052	39.882
	2.0	5.6329	12.023	22.002	26.435	33.461	40.076	46.647	57.521
H^*	1.0	8.1858	16.51	17.434	27.704	29.806	30.449	41.248	43.232
	1.5	12.673	22.831	31.417	37.465	42.773	54.98	57.353	65.759
	2.0	19.391	30.276	44.168	55.839	58.865	71.782	75.814	92.654
I^*	1.0	5.6979	13.438	13.859	23.234	25.468	26.336	36.351	37.51
	1.5	8.7584	17.481	25.557	30.768	36.252	47.174	49.331	57.007
	2.0	13.273	22.568	34.981	45.035	49.436	59.743	65.969	79.006

A^* support condition, B^* CCCC, D^* SSSS, E^* CCSS, G^* CCFF, H^* CCCS, I^* CSSS

Table 18 Dimensionless natural frequencies $\beta_1 = \omega a^2(\rho h/D)^{\frac{1}{2}}$ of a rectangular plate with one-side curved edge

a/b	Support Condition	1	2	3	4	5	6
1.0	CCCC	10.471	20.853	21.489	34.578	35.410	37.013
	SSSS	5.2873	13.573	14.1498	25.551	25.739	27.535
	CCSS	7.1094	15.833	17.35	28.316	29.977	31.861
1.5	CCCC	17.384	28.241	39.321	45.837	54.586	65.941
	SSCC	13.436	23.9	33.436	39.953	48.038	58.719
	SSSS	8.5009	17.35	26.163	31.995	40.086	49.699
2.0	CCCC	27.465	38.945	53.366	70.813	71.69	90.397
	SSSS	13.149	22.538	34.764	47.344	51.348	65.425
	CCSS	19.257	29.368	41.917	57.363	58.872	75.584

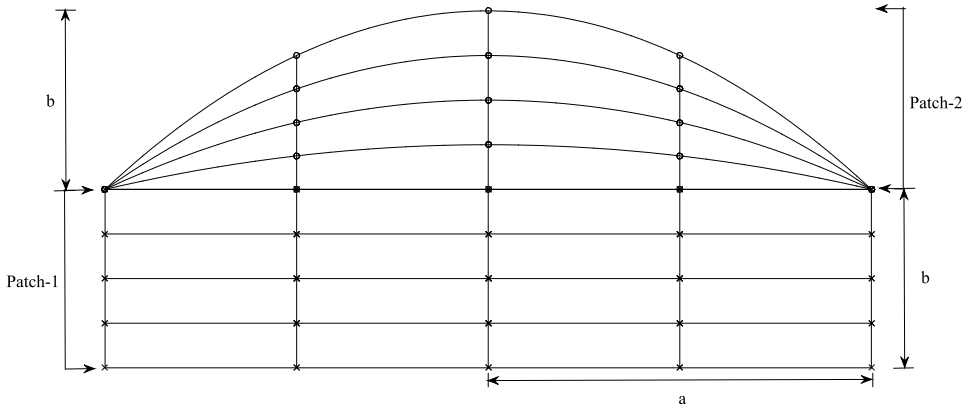

Fig. 60 A typical rectangular plate with one-side curved edge consisting of a rectangular portion as patch-1 (4 × 4 mesh) and the remaining as patch-2 (4 × 4 mesh)

Conflict of Interest On behalf of all the authors, the corresponding author states that there is no conflict of interest.

References

1. Mishra BP, Barik M (2020) NURBS-Augmented finite element method for static analysis of arbitrary plates. Comput Struct 232:105869 (**Mechanics and Modelling of Materials and Structures**)
2. Mishra BP, Barik M (2019) NURBS-Augmented finite element method for stability analysis of arbitrary thin plates. Eng Comput 35(2):351–362
3. Mukhopadhyay M (1979) A semi-analytic solution for free vibration of annular sector plates. J Sound Vib 63:87–95
4. Cheung YK, Tham LG, Li WY (1988) Free vibration and static analysis of general plate by spline finite strip. Comput Mech 3:187–197
5. Bert CW, Malik M (1996) The differential quadrature method for irregular domains and application to plate vibration. Int J Mech Sci 38:589–606
6. Barik M, Mukhopadhyay M (1998) Finite element free flexural vibration analysis of arbitrary plates. Finite Elem Anal Des 29:137–151
7. Barik M (1999) Finite element static, dynamic and stability analyses of arbitrary stiffened plates. Ph.D. thesis, I.I.T., Kharagpur
8. Lee SJ (2004) Free vibration analysis of plates by using a four-node finite element formulated with assumed natural transverse shear strain. J Sound Vib 278(3):657–684
9. Liew KM, Wang J, Ng TY, Tan MJ (2004) Free vibration and buckling analyses of shear-deformable plates based on FSDT meshfree method. J Sound Vib 276:997–1017
10. Cottrell JA, Reali A, Bazilevs Y, Hughes TJR (2006) Isogeometric analysis of structural vibrations. Comput Methods Appl Mech Eng 195:5257–5296
11. Reali A (2006) An isogeometric analysis approach for the study of structural vibrations. J Earthq Eng 10(sup001):1–30
12. Hota SS, Padhi P (2007) Vibration of plates with arbitrary shapes of cut-outs. J Sound Vib 302:1030–1036
13. Sevilla R, Fernández S, Huerta A (2008) NURBS-enhanced finite element method (NEFEM). Int J Numer Methods Eng 76:56–83
14. Lu J (2009) Circular element: isogeometric elements of smooth boundary. Comput Methods Appl Mech Eng 198:2391–2402
15. Xing Y, Liu B (2009) High-accuracy differential quadrature finite element method and its application to free vibrations of thin plate with curvilinear domain. Internat J Numer Methods Eng 80:1718–1742
16. Zhong H, Yue ZG (2012) Analysis of thin plates by the weak form quadrature element method. Sci. China Phys Mech 55:861–871
17. Civalek Ö (2010) Use of eight-node curvilinear domains in discrete singular convolution method for free vibration analysis of annular sector plates with simply supported radial edges. J Vib Control 16:303–320
18. Akgöz B, Civalek Ö (2016) Static and dynamic response of sector-shaped graphene sheets. Mech Adv Mater Struct 23:432–442
19. Wang D, Xuan J (2010) An improved NURBS-based isogeometric analysis with enhanced treatment of essential boundary conditions. Comput Methods Appl Mech Eng 199:2425–2436

20. Bazilevs Y, Calo VM, Cottrell JA, Evans JA, Hughes TJR, Lipton S, Scott MA, Sederberg TW (2010) Isogeometric analysis using T-splines. Comput Methods Appl Mech Eng 199(5):229–263
21. Hughes TJR, Reali A, Sangalli G (2010) Efficient quadrature for NURBS-based isogeometric analysis. Comput Methods Appl Mech Eng 199(5):301–313
22. Costantini P, Manni C, Pelosi F, Sampoli LM (2010) Quasi-interpolation in isogeometric analysis based on generalized B-splines. Comput Aided Geomet Des 27(8):656–668
23. de Falco C, Reali A, Vázquez R (2011) GeoPDEs: a research tool for isogeometric analysis of PDEs. Adv Eng Softw 42(12):1020–1034
24. Bui TQ, Nguyen MN (2011) A moving Kriging interpolation-based meshfree method for free vibration analysis of Kirchhoff plates. Comput Struct 89:380–394
25. Schmidt R, Wüchner R, Bletzinger K-U (2012) Isogeometric analysis of trimmed NURBS geometries. Comput Methods Appl Mech Eng 241–244:93–111
26. Ghasemzadeh H, Shojaee S, Ghorashi SS, Valizadeh N, Mohammadi S (2012) Analysis of thin plates by a combination of isogeometric analysis and the Lagrange multiplier approach. Comput Methods Civ Eng 3(2):47–66
27. Tran LV, Ferreira AJM, Nguyen-Xuan H (2013) Isogeometric analysis of functionally graded plates using higher order shear deformation theory. Compos Part B 51:368–383
28. Lu J, Yang G, Ge J (2013) Blending NURBS and Lagrangian representations in isogeometric analysis. Comput Methods Appl Mech Eng 257:117–125
29. Valizadeh N, Natrajan S, Gonzalez-Estrada OA, Rabczuk T, Bui TQ, Bordas SPA (2013) NURBS-based finite element analysis of functionally graded plates: static bending, vibration, buckling and flutter. Compos Struct 99:309–326
30. Nguyen-Xuan H, Tran LV, Thai CH, Kulasegaram S, Bordas SPA (2014) Isogeometric analysis of functionally graded plates using a refined plate theory. Compos B 64:222–234
31. Yin S, Hale JS, Yu T, Bui TQ, Bordas SPA (2014) Isogeometric analysis of functionally graded plates using a refined plate theory. Compos Struct 118:121–138
32. Jüttler B, Langer U, Mantzaflaris A, Moore SE (2014) Geometry + simulation modules: implementing isogeometric analysis. Proc Appl Math Mech 14(1):961–962
33. Nguyen KD, Nguyen-Xuan H (2015) An isogeometric finite element approach for three-dimensional static and dynamic analysis of functionally graded material plate structures. Compos Struct 132:423–439
34. Tran LV, Ly HA, Lee J, Wahab MA, Nguyen-Xuan H (2015) Vibration analysis of cracked FGM plates using higher-order shear deformation theory and extended isogeometric approach. Int J Mech Sci 96–97:65–78
35. Vázquez R (2016) A new design for the implementation of isogeometric analysis in octave and Matlab: GeoPDEs 3.0. Comput Math Appl 72(3):1059–1127
36. Massarwi F, Elber G (2016) A B-spline based framework for volumetric object modeling. Comput Aided Des 78:36–47
37. Liu C, Liu B, Zhao L, Xing Y, Ma C, Li H (2016) A differential quadrature hierarchical finite element method and its applications to vibration and bending of Mindlin plates with curvilinear domains. Int J Numer Methods Eng 109:174–197
38. Liu B, Xing Y, Wang Z, Lu X, Sun H (2017) Non-uniform rational Lagrange functions and its applications to isogeometric analysis of in-plane and flexural vibration of thin plates. Comput Methods Appl Mech Eng 321:173–208
39. Civalek Ö (2017) Free vibration of carbon nanotubes reinforced (CNTR) and functionally graded shells and plates based on FSDT via discrete singular convolution method. Compos B 111:45–59
40. Marussig B, Hughes TJR (2018) A review of trimming in isogeometric analysis: challenges, data exchange and simulation aspects. Arch Comput Methods Eng 25:523–554
41. Guan X, Tang J, Shi D, Shuai C, Wang Q (2018) A semi-analytical method for transverse vibration of sector-like thin plate with simply supported radial edges. Appl Math Model 60:48–63
42. Antolin P, Buffa A, Martinelli M (2019) Isogeometric analysis on V-reps: first results. Comput Methods Appl Mech Eng 355:976–1002
43. Liu T, Hu G, Wang A, Wang Q (2019) A unified formulation for free in-plane vibration of arbitrary-shaped straight-sided quadrilateral and triangular thin plates. Appl Acoust 155:407–422
44. Alihemmati J, Beni YT (2020) Developing three-dimensional mesh-free Galerkin method for structural analysis of general polygonal geometries. Eng Comput 36:1059–1068
45. Sahoo PR, Barik M (2020) Free vibration analysis of stiffened plates. J Vib Eng Technol 8(6):869–882. https://doi.org/10.1007/s42417-020-00196-4
46. Sahoo PR, Barik M (2020) A numerical investigation on the dynamic response of stiffened plated structures under moving loads. Structures 28:1675–1686. https://doi.org/10.1016/j.istruc.2020.09.056
47. Sahoo PR, Barik M (2021) Free vibration analysis of curved stiffened plates. J Vib Eng Technol. https://doi.org/10.1007/s42417-021-00284-z
48. Khalafi V, Fazilati J (2022) Panel flutter analysis of cracked functionally graded plates in yawed supersonic flow with thermal effects. Appl Math Model 101:259–275. https://doi.org/10.1016/j.apm.2021.07.043
49. Khalafi V, Fazilati J (2018) Parametric instability behavior of tow steered laminated quadrilateral plates using isogeometric analysis. Thin-Walled Struct 133:96–105
50. Khalafi V, Fazilati J (2021) Panel flutter analysis of perforated plate repaired by vscl bonded patch using the multi-patch iga approach. Thin-Walled Struct 169: 108465. https://doi.org/10.1016/j.tws.2021.108465. https://www.sciencedirect.com/science/article/pii/S026382312100598X
51. Dynamic analysis of the composite laminated repaired perforated plates by using multi-patch iga method. Chin J Aeronaut **34**(1), 266–280 (2021). https://doi.org/10.1016/j.cja.2020.09.038
52. Khalafi V, Fazilati J (2018) Supersonic panel flutter of variable stiffness composite laminated skew panels subjected to yawed flow by using nurbs-based isogeometric approach. J Fluids Struct 82:198–214. https://doi.org/10.1016/j.jfluidstructs.2018.07.002
53. Khalafi V, Fazilati J (2019) Effects of embedded perforation geometry on the free vibration of tow-steered variable stiffness composite laminated panels. Thin-Walled Struct 144: 106287. https://doi.org/10.1016/j.tws.2019.106287. https://www.sciencedirect.com/science/article/pii/S0263823119301120
54. Liu T, Hu G, Wang A, Wang Q (2019) A unified formulation for free in-plane vibrations of arbitrarily-shaped straight-sided quadrilateral and triangular thin plates. Appl Acoust 155:407–422
55. Khalafi V, Fazilati J (2021) Dynamic analysis of the composite laminated repaired perforated plates by using multi-patch iga method. Chin J Aeronaut 34(1):266–280
56. Do V, Lee C (2019) Free vibration analysis of fgm plates with complex cutouts by using quasi-3d isogeometric approach. Int J Mech Sci 159:213–233
57. Hughes TJR, Cottrell JA, Bazilevs Y (2005) Isogeometric analysis: CAD, finite elements, NURBS, exact geometry and mesh refinement. Comput Methods Appl Mech Eng 194:4135–4195
58. Shojaee S, Izadpanah E, Valizadeh N, Kiendl J (2012) Free vibration analysis of thin plates by using a NURBS-based Isogeometric approach. Finite Elem Anal Des 61:23–34
59. Shojaee S, Valizadeh N, Izadpanah E, Bui T, Vu TV (2012) Free vibration and buckling analysis of laminated composite plates

using the NURBS-based Isogeometric finite element method. Compos Struct 94:1677–1693
60. Shojaee S, Izadpenah E, Haeri A (2012) Imposition of essential boundary conditions in isogeometric analysis using the Lagrange multiplier method. Int J Optim Civ Eng 2:247–271
61. Wang D, Liu W, Zhang H (2015) Superconvergent isogeometric free vibration analysis of Euler-Bernoulli beams and Kirchhoff plates with new higher order mass matrices. Comput Methods Appl Mech Eng 286:230–267
62. Chen T, Mo R, Gong ZW (2012) In: Frontiers of manufacturing and design science II, Applied Mechanics and Materials, vol. 121 (Trans Tech Publications, 2012), pp. 2779–2783. https://doi.org/10.4028/www.scientific.net/AMM.121-126.2779
63. Chang F, Wang W, Liu Y, Qu Y (2015) In: International Conference on computer science and applications (CSA) (2015), pp 213–217. https://doi.org/10.1109/CSA.2015.53
64. Wang D, Xuan J (2010) An improved NURBS-based isogeometric analysis with enhanced treatment of essential boundary conditions. Comput Methods Appl Mech Eng 199(37):2425–2436
65. Adini A, Clough RW (1961) Analysis of plate bending by the finite element method. Report to National Science Foundation, U.S.A., G.7337
66. Mishra BP. Barik M (2016) In: Insights and innovations in structural engineering, mechanics and computation: Proceedings of the Sixth International Conference on Structural Engineering, Mechanics and Computation, (ed. Zingoni, A.), 5–7 September 2016, Cape Town, South Africa. (Taylor & Francis Group, 2016), pp 516–521
67. Mishra BP, Barik M (2021) Free flexural vibration of thin stiffened plates using nurbs-augmented finite element method. Structures 33:1620–1632
68. Nguyen VP, Anitescu C, Bordas SPA, Rabczuk T (2015) Isogeometric analysis: an overview and computer implementation aspects. Math Comput Simul 117:89–116
69. Cottrell JA, Hughes TJR, Reali A (2007) Studies of refinement and continuity in Isogeometric structural analysis. Comput Methods Appl Mech Eng 196:4160–4183
70. Corr RB, Jennings E (1976) A simultaneous iteration algorithm for solution of symmetric eigenvalue problem. Int J Numer Methods Eng 10:647–663
71. Zienkiewicz OC, Taylor RL (1989) The finite element method, 4th edn. McGraw-Hill Book Co., London
72. Leissa AW (1973) The free vibration of rectangular plates. J Sound Vib 31(3):257–293
73. Malik M, Bert CW (1998) Three-dimensional elasticity solutions for free vibrations of rectangular plates by the differential quadrature method. Int J Solids Struct 35(3):299–318
74. Lim CW, Lü CF, Xiang Y, Yao W (2009) On new symplectic elasticity approach for exact free vibration solutions of rectangular kirchhoff plates. Int J Eng Sci 47(1):131–140
75. Ramu I, Mohanty SC (2012) Study on free vibration analysis of rectangular plate structures using finite element method. Proc Eng 38: 2758–2766. https://doi.org/10.1016/j.proeng.2012.06.323. https://www.sciencedirect.com/science/article/pii/S1877705812022369. International Conference on modelling optimization and computing
76. Bui QT, Nguyen NM (2011) A moving Kriging interpolation-based meshfree method for free vibration analysis of Kirchhoff plates. Comput Struct 89:380–394
77. Hinton E (1988) Numerical Methods and Software for Dynamic Analysisof Plates and Shells. Pineridge Press, Swansea
78. Bui QT, Guyen NM (2011) A moving Kriging interpolation-based mesh-free method for free vibration analysis of Kirchoff plates. Comput Struct 89:380–394